Astronomy & Astrophysics manuscript no. v746cas
April 20, 2017

An improved model of the triple system V746 Cas with a bipolar magnetic field associated with the tertiary ⋆

P. Harmanec[1], P. Mayer[1], P. Zasche[1], L. Kotková[2], J.A. Nemravová[1], R.J. Dukes[3], M. Brož[1], D. Korčáková[1], M. Šlechta[2], E. Kıran[4,1], R. Kříček[1], and J. Juryšek[1,5]

[1] Astronomical Institute of the Charles University, Faculty of Mathematics and Physics, V Holešovičkách 2, CZ-180 00 Praha 8, Czech Republic
[2] Astronomical Institute, Czech Academy of Sciences, CZ-251 65 Ondřejov, Czech Republic
[3] Department of Physics and Astronomy, The College of Charleston, Charleston, SC 29424, USA
[4] University of Ege, Department of Astronomy & Space Sciences, 35 100 Bornova - İzmir, Turkey
[5] Institute of Physics, Czech Academy of Sciences, Na Slovance 1999/2, CZ-182 21 Praha 8, Czech Republic

Received April 20, 2017; accepted

ABSTRACT

V746 Cas is known to be a triple system composed of a close binary with a period of $25\overset{d}{.}4$ and a distant third component in a 170 yr (62000 d) orbit. The object was also reported to exhibit multiperiodic light variations with periods from $0\overset{d}{.}83$ to $2\overset{d}{.}50$ on the basis of which it was classified as a slowly pulsating B star. Interest in further investigation of this system was raised by a recent detection of the variable magnetic field. Analysing radial velocities from four instruments and earlier published data we arrived at the following conclusions: (1) The optical spectrum is dominated by the lines of the B-type primary ($T_{\rm eff} \sim 15850(400)$ K), contributing 70 % of light in the optical region, and a slightly cooler B tertiary ($T_{\rm eff} \sim 14920(490)$ K). The lines of the low-mass secondary are below our detection threshold; we estimate it could be a normal A star. (2) We resolved the ambiguity in the value of the inner binary period and arrived at the following linear ephemeris $T_{\rm super.\,conj.}$ = HJD 2443838.78(81) + $25\overset{d}{.}41569(42) \times E$. (3) Even in the absence of binary eclipses, we can constrain the orbital inclination of the inner orbit: $70° < i < 85°$. (4) The intensity of the magnetic field undergoes a sinusoidal variation in phase with one of the known photometric periods, namely $2\overset{d}{.}503867(19)$, which we identify with the rotational period of the tertiary; this is consistent with corresponding $v \sin i = 72(4)$ km s^{-1}. (5) The observed line profiles seem affected by rapid line-profile variations, probably related to the dominant photometric $1\overset{d}{.}0649524(40)$ period, which we tentatively identify with the rotational period of the broad-lined B-type primary, having $v \sin i = 179(6)$ km s^{-1}. (6) If our interpretation of photometric periods is confirmed, the classification of the object as a slowly pulsating B star should be revised.

Key words. Stars: binaries: spectroscopic – stars: massive – stars: fundamental parameters – stars: individual: V746 Cas = HD 1976; HR 96 = HD 2054

1. Introduction

While the nature of global magnetic fields in late-type stars with convective envelopes seems to be – at least in principle – understood as a consequence of the dynamo mechanism, the origin of organized magnetic fields detected in some O and B stars is less obvious. Given the large progress in the instrumentation allowing the detection of even weak magnetic fields, it is understandable that a very systematic search for the presence of magnetic fields among WR, O, B, and Be stars had recently be conducted by a large team of collaborators. This project known as MiMES (Magnetism in MassivE Stars) was conducted between 2008 and 2013 and the first summary report was published by Wade et al. (2016). These authors mention that unlike the magnetic fields of late-type stars, the magnetic fields of hot stars do not show any clear correlations with the basic stellar properties such as their mass or rate of rotation. We note that there has been growing realisation in recent years that a large fraction of O and B stars are binaries or even multiple systems, which must have significant impact on the understanding of their properties (see, e.g. Chini et al. 2012; de Mink et al. 2013). We believe that the role of multiplicity in the magnetism of hot stars is worth of consideration. Recently, Neiner et al. (2014) reported one preliminary result of the MiMES survey: the discovery of magnetic field of the triple system V746 Cas. Since the properties of this system were not well known, it prompted us to this study.

V746 Cas (HD 1976, HR 91, BD+51°62, HIP 1921, Boss 67) is a bright ($V = 5\overset{m}{.}6$) B5IV star. Its radial-velocity (RV) variations were discovered by Adams (1912) and confirmed by Plaskett & Pearce (1931). Blaauw & van Albada (1963) derived RVs from a new series of McDonald spectra and published the first orbital elements – see Table 1. Besides their spectra, they also used the DAO spectra. Abt (1970) published six older Mt. Wilson RVs, which partly overlap with those published by Adams (1912). Abt et al. (1990) measured RVs of 20 new KPNO spectra and published another set of elements, deriving a period of $25\overset{d}{.}44 \pm 0\overset{d}{.}03$. Their solution is based solely on the KPNO RVs but the authors claim that it fits also the older Mt. Wilson, DAO, and McDonald RVs. McSwain et al. (2007) analysed their 15 new KPNO RVs along with earlier published data and found two comparable periods near $25\overset{d}{.}4$ and $27\overset{d}{.}6$. We note that these two periods are 1 yr aliases of each other. McSwain et al. (2007) preferred the shorter period and obtained another solution, this time

⋆ Based on observations from the Ondřejov, Haute Provence, Bernard Lyot, ESO Hipparcos and Mercator Observatories.

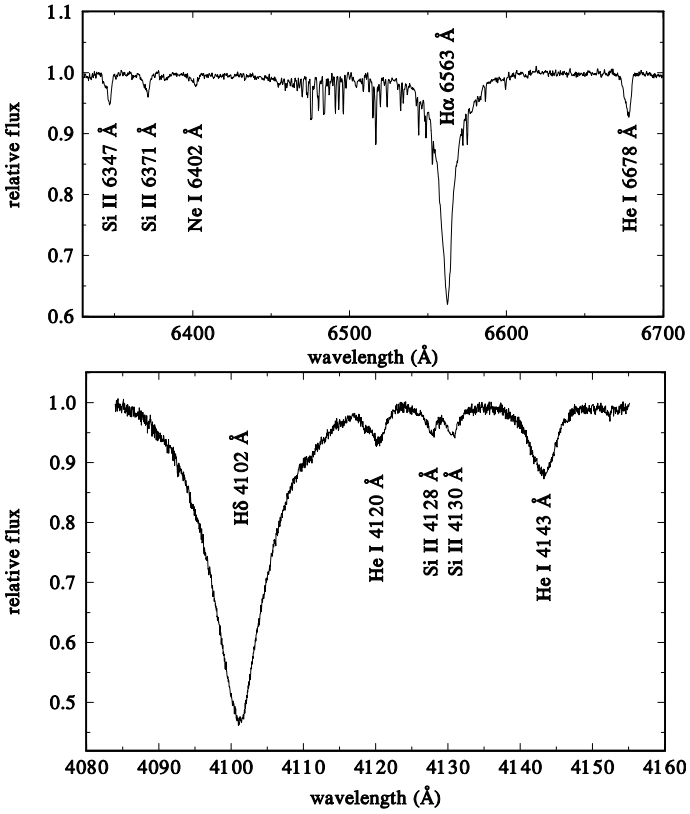

Fig. 1. *Top:* The Ondřejov spectrum taken on RJD 56928.3090 is shown, with identification of several stronger spectral lines. All sharp lines in the vicinity of Hα are telluric or weak interstellar lines. *Bottom:* The Haute Provence Aurelie spectrum taken on RJD 51011.5748, again with identification of stronger lines.

Table 1. Previously published orbital solutions.

Element	1	2	3
P (d)	27.8	25.44(3)	25.4176(4)
$T_{\rm periastr.}$(RJD)	not given	43840.3(3)	35783.5(1)
e	0.2	0.14(9)	0.12(3)
ω (°)	140	165(5)	172(2)
K (km s^{-1})	30	23.4(1.9)	23.6(7)
γ (km s^{-1})	−18.	−15.8(1.3)	−9.7(5)
rms (km s^{-1})	not given	4.5	4.81
No. of RVs	16	20	15+32

Notes. All epochs are in RJD=HJD-2400000.0; rms is the rms of 1 observation of unit weight.
Solutions Nos.: 1...Blaauw & van Albada (1963), 2...Abt et al. (1990), 3...McSwain et al. (2007)

based on most of previously published RVs, which is also given in Table 1.

The first attempt to detect the spectral lines of the secondary was reported by Gómez & Abt (1982). They studied 160 Å long CCD spectra in two wavelength regions: one containing He I 5876 Å and the Na I doublet at 5889 and 5895 Å, and the other containing the Si II doublet at 6347 and 6371 Å, Ne I 6402 Å line and several Fe II, Fe I, and Ca I lines, to be able to restrict possible spectral class of the secondary. They did not

Table 2. Journal of RV data sets

Spg. No.	Time interval (RJD)	No. of RVs	Source
1	19026.89–23004.70	7	A
2	24010.41–24891.13	6	B
3	35795.62–35833.55	16	C
4	43411.86–44231.62	20	D
5	53657.79–53696.79	15	E
6	50967.59–51099.45	17	F
7	52538.56–53026.28	3	F
8	56175.56–56214.42	13	F
9	56746.65–57328.69	41	F

Notes. Column "Spg. No.": 1...Mount Wilson Solar Observatory 1.52 m reflector, 3-prism spg; 2...Dominion Astrophysical Observatory 1.88 m reflector, prism spg.; 3...McDonald 2.08 m reflector, coudé grating spg. 34 Å mm^{-1}; 4...Kitt Peak 1 m coudé feed telescope, grating spg. 16.9 Å mm^{-1}; 5...Kitt Peak 2.1 m reflector, grating spg.; 6...Haute Provence 1.52 m reflector, Aurelie linear electronic spg.; 7...Haute Provence 1.52 m reflector, Elodie echelle spg.; 8...Bernard Lyot 2 m reflector, echelle spg.; 9...Ondřejov 2.0 m reflector, coudé grating spg. 17.2 Å mm^{-1}.
Column "Source": A...Adams (1912); Abt (1970); B...Plaskett & Pearce (1931); C...Blaauw & van Albada (1963); D...Abt et al. (1990); E...McSwain et al. (2007); F...This paper.

show the actual line profiles and published only a few comments. They concluded that the spectral type of the secondary must be earlier than F6, and suspected presence of a possible weak secondary component in the He I 5876 Å line.

V746 Cas is also the brighter member of the visual system ADS 328. Doboco & Andrade (in Doboco & Ling 2005) derived the orbit of the wide pair with a period of 169.29 yrs (61832 d), semimajor axis 0.″214, eccentricity 0.163, inclination 64.°8, argument of periastron 311.°8 and periastron passage at 1955.06 (JD 2435130). The distant component B is for some 0.$^{\rm m}$9 fainter than V746 Cas.

The light variability of V746 Cas in the range from 5.$^{\rm m}$54 to 5.$^{\rm m}$56 was discovered by the Hipparcos team (Perryman & ESA 1997) and several investigators reported the presence of two principal periods, 1.$^{\rm d}$065 and 2.$^{\rm d}$504 and alternatively also a few additional ones (for instance Waelkens et al. 1998; Andrews & Dukes 2000; De Cat et al. 2007; Dukes et al. 2009, see sect. 4 for more detailed account). They all classified the object as a slowly pulsating B-type star (SPB).

Neiner et al. (2014) reported the discovery that the line spectra of V746 Cas are composed of a narrow component, for which they found clear signatures of a magnetic field, and a broad component, much more variable in RV. They identified the narrow lines and the magnetic field with the primary and the broad-line component with the secondary of the 25.$^{\rm d}$4 binary, concluding that the lines of the distant tertiary are not seen in the spectra. They admitted, however, that the narrow-lined star could also be the visual tertiary or a combination of the primary and tertiary.

Our initial motivation to this study was to resolve the remaining ambiguity in the value of the orbital period. We started to collect new CCD spectra in the red spectral region. Their subsequent analysis led us to a more complex investigation and,

hopefully a better understanding of this remarkable triple system, which we report here.

2. Available observational data and their initial reductions

2.1. Spectroscopy

Our observational material consists of 41 Ondřejov CCD spectra secured in the years 2014 – 2015 (S/N 160–300; three underexposed spectra with 27, 37, and 100), 17 OHP Aurelie spectra with S/N 130-230, the first one of 36 only (Gillet et al. 1994), which were obtained and studied by Mathias et al. (2001), 3 archival OHP Elodie spectra with S/N 270–280 in the red parts of the spectra (Moultaka et al. 2004), and 13 publicly available echelle spectra from the Bernard Lyot telescope with S/N greater than 200 in the red parts of the spectra (Petit et al. 2014). The initial reduction of all Ondřejov spectra (bias subtraction, flat-fielding, creation of 1-D spectra, and wavelength calibration) was carried out in `IRAF`. For the Bernard Lyot and OHP Elodie spectra, extracted from public databases, we adopted the original reductions, verifying that the zero point of the wavelength scale was corrected via telluric lines as it was the case for the Ondřejov spectra. The story was a more complicated with the Aurelie spectra, which are not available from public archives. Dr. P. Mathias kindly provided us with the old DAT tapes, which were reconstructed in Prague. Their new reduction was carried out with the help of simple dedicated programs, the wavelength calibration being carried out with the program `SPEFO` (Horn et al. 1996; Škoda 1996), namely the latest version 2.63 developed by Mr. J. Krpata. Median values of each corresponding sets of offsets and flat spectra were used.

Rectification and removal of residual cosmics and flaws for all sets of spectra were carried out in `SPEFO`.

We first extracted the red parts of the Elodie and Bernard Lyot spectra (~6360 – 6740 Å) to have the same spectral region as that covered by the Ondřejov spectra. One Ondřejov spectrum is shown in Fig. 1. One can see – as it has already be noted by Neiner et al. (2014) – that the line profiles are not symmetric but contain broad and narrow components, the broad one varying in RV over a large velocity range. To this, we mention the possibility that the profiles could also be affected by subfeatures, related to rapid light and line-profile variations and moving across the line profiles due to stellar rotation. For all Elodie and Bernard Lyot spectra, we also extracted the blue, green, and yellow parts of the spectra over the wavelength range from 4000 to 6360 Å. We also extracted the Aurelie spectra, which cover the wavelength range from 4095 to 4155 Å.

Finally, we also collected radial-velocity (RV) measurements obtained by several investigators and published in the literature. The journal of all available RVs is in Table 2 and all individual RVs are in Tab. A.1 for the data from the literature. Whenever not available in the original source, we converted the dates of observations to HJDs. For brevity, we use *reduced* Julian dates

$$\mathrm{RJD} = \mathrm{HJD} - 240000.0$$

everywhere in this paper. Abt (1970) published 6 RVs from Mount Wilson secured between December 1910 and November 1921. They include RVs published by Adams (1912) with the exception of the very first observation secured on 1910 Dec. 21. We therefore adopted the first RV from Adams (1912) and all remaining Mount Wilson RVs (spg. 1) from Abt (1970).

Table 3. Improved visual orbit of V746 Cas.

Element	Value with rms error
P (d/yr)	62004 ± 1202/169.76 ± 3.29
$T_{\mathrm{periastr.}}$(RJD)	34613 ± 820
e	0.176 ± 0.023
ω (°)	308.2 ± 9.4**
Ω (°)	29 ± 12
i (°)	64 ± 16
a (mas)	211 ± 97
$M_1 + M_2 + M_3$ ($M_\odot$)	9.34(range 5.50–17.8)*

Notes. *) Assuming a revised Hipparcos parallax of 0.″00326±0.″00063 after van Leeuwen (2007a,b). **) The argument of periastron refers to the visual tertiary. For the close binary it would be 128.°2, of course.

2.2. Standard RV measurements

In effort to resolve the problem of the true orbital period and to obtain reliable orbital elements, we first tested several techniques of RV measurements. For the most numerous set of the red spectra, we measured the two strongest lines, Hα and He I 6678 Å in `SPEFO`. This program displays direct and flipped traces of the line profiles superimposed on the computer screen that the user can slide to achieve a precise overlapping of the parts of the profile of whose RV one wants to measure. We separately measured the line cores and outer line wings. We note that two of the Ondřejov spectra (RJDs 56920 and 57228) are underexposed and we could only measure the RVs of the wings of Hα. Alternatively, the RVs of He I 6678 Å line were also measured via a fit with two Gaussian profiles. These RV measurements are listed in Table A.2. For the Aurelie spectra, we also measured RVs of the broad wings of the He I 4144 Å line and these measurements are in Tab. A.3 in Appendix A. **To estimate the errors of `SPEFO` measurements of individual lines, we repeated these measurements independently three times and used the mean RVs and the rms of the mean.**

For the Elodie and Bernard Lyot spectra, we also measured RVs of the following stronger lines in `SPEFO`: He I 4009, 4143, 4471, 4713, 4922, 5016, 5047, and 5876 Å, C II 4267 Å, and Mg II 4481 Å. We have not used the He I 4026 Å, 4120 Å, and 4387 Å lines, since the first is affected by an inter-order jump in all Bernard Lyot spectra, while the profiles of the other two are affected by strong blends in their neighbourhood. Finally, for Aurelie spectra we measured RVs of Hδ and He I 4143 Å. All these RVs were used for exploratory purposes and determination of a new ephemeris. The final set of Elodie and Bernard Lyot RVs was obtained from the comparison of observed and synthetic spectra with the program `PYTERPOL` – see sect. 3.3 below – and these RVs are in Table A.4 in Appendix A.

2.3. Photoelectric observations and their homogenisation

There are three principal sets of photoelectric observations suitable for period analyses:

1. The Hipparcos H_{p} observations (Perryman & ESA 1997),
2. the *uvby* observations from the Four-College APT secured by one of us; a subset of these observations had already been analysed by Dukes et al. (2009), and

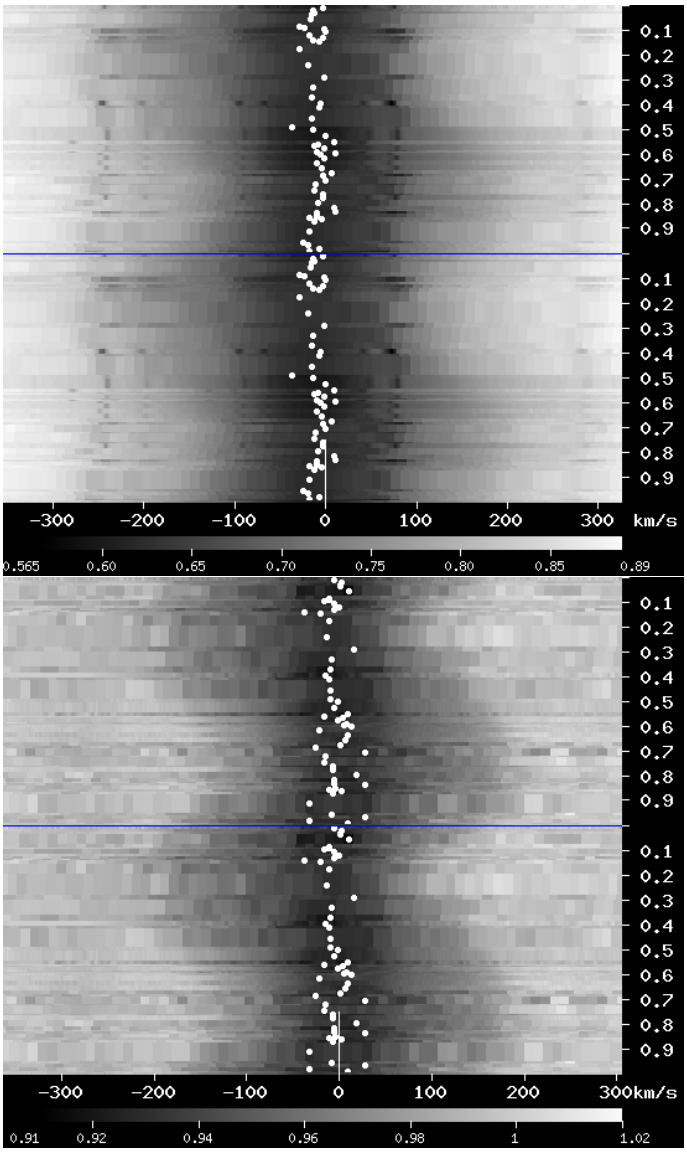

Fig. 2. Dynamical spectra plotted vs. orbital phase of the $25\overset{\mathrm{d}}{.}416$ period with phase zero at superior conjunction. Lines of Hα (top panel) and He I 6678 Å (bottom panel) are shown. The white dots denote the RV position of the deepest point of each line profile to show that the position of line cores does not vary with the $25\overset{\mathrm{d}}{.}416$ period.

3. Geneva 7-C observations obtained and studied by De Cat et al. (2004) and De Cat et al. (2007).

One of us, R.J. Dukes, was able to recover the APT *uvby* observations, actually a more numerous data set than that used in his published studies. It was deemed useful to repeat the period analysis with a complete and homogenised set of the data. The yellow observations (H_p and Geneva V magnitudes converted to Johnson V, and Strömgren y), are the most numerous and represent the best set for the analysis. More details on the data processing and their homogenisation can be found in Appendix C, where also the journal of these observations is in Tab. C.1. After the removal of data from non-photometric nights, we are left with 2060 individual yellow observations spanning an interval of nearly 9800 d.

2.4. Speckle interferometry and the visual orbit

Adding one additional speckle-interferometric observation from 2007 (Mason et al. 2009) to the existing body of visual observations of V746 Cas, we derived an improved visual orbit of the third body. Our solution confirmed and only slightly improved the orbit published by Docobo and Andrade (see Doboco & Ling 2005). It is summarised in Table 3.

3. Properties of the triple system

Figure 2 shows dynamical spectra for the Hα and He I 6678 Å line vs. phase of the $25\overset{\mathrm{d}}{.}416$ period. One can see the orbital motion in the line wings of both lines. In contrast to it, the line cores indicate a more or less constant RV. We also note that there is no indication of an antiphase RV variation expected for the secondary in the $25\overset{\mathrm{d}}{.}416$ orbit. This means that the bulk of the line cores *is not* associated with *the primary* as suggested by Neiner et al. (2014) but with *the tertiary* of the visual orbit.

3.1. Period analysis of RVs

As mentioned earlier, we measured separately RVs of the broad and narrow parts of Hα and He I 6678 Å lines. We immediately noted – in accord with Neiner et al. (2014) – that the range of RV variations is smaller for the narrow parts of the lines. We preliminary verified that the RVs of the wide parts of the lines vary with the known ∼ 25 d period. This is not so for the RVs of the line cores. They do not exhibit any anti-phase orbital variations with the $25\overset{\mathrm{d}}{.}4$ period. In fact, the SPEFO RVs of the line cores of the Balmer lines seemingly follow the ∼ 25 d RV curve of the wide parts of the lines, *in phase with the wide wings but with a strongly reduced amplitude*. This implies that they do not belong to the secondary in the 25 d orbit but to the distant tertiary, with nearly constant RV. Their apparent RV changes are caused only by the strong line blending of the lines of the primary and tertiary.

To resolve the question of the true value of the orbital period of closer pair, we calculated PDM periodograms (Stellingwerf 1978) for individual data subsets. They are shown in Fig. 3. It is immediately seen that neither Blaauw & van Albada (1963) not McSwain et al. (2007) RVs alone are able to restrict the value of the orbital period. Blaauw & van Albada (1963) were obviously aware of the limitations of their data set since they estimated that the uncertainty of the $27\overset{\mathrm{d}}{.}8$ period does not exceed 1 day. The time interval covered by their own observations is shorter than two orbital periods. We also note that the first data set from spectrograph 1, though spanning a long time interval, is probably of limited accuracy and cannot be used to the determination of a unique period.

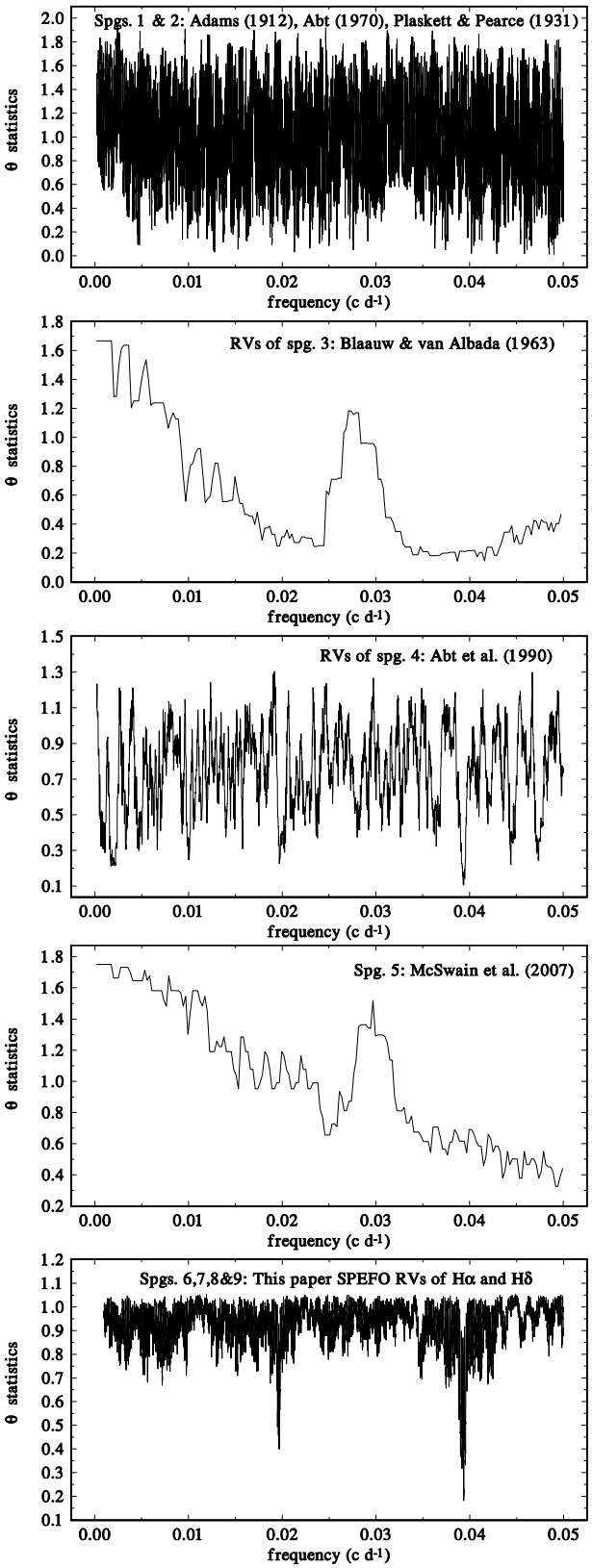

Fig. 3. Stellingwerf (1978) θ statistics periodograms for several data sets of RVs published by various authors, and the SPEFO RVs of the outer wings of the Hα and Hδ lines.

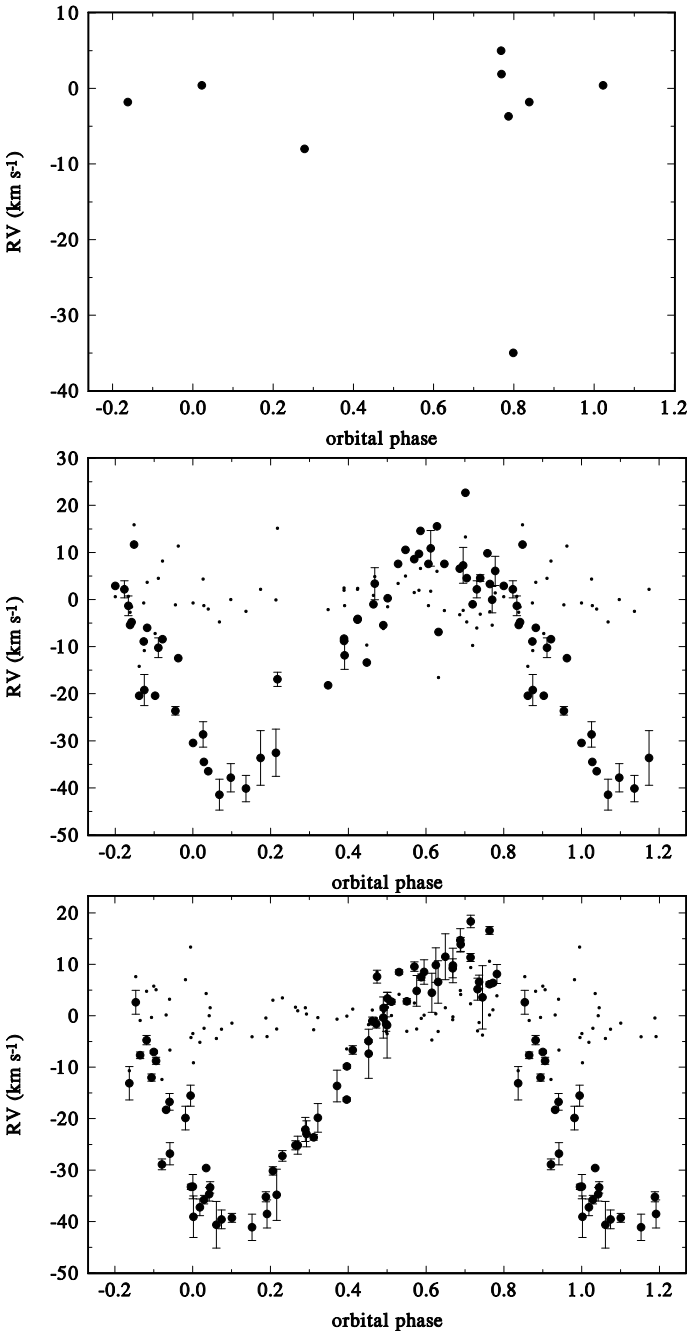

Fig. 4. *Top:* A phase plot of the earliest spectrograph 1 (Mount Wilson) RVs. *Middle:* A phase plot of all file 2 to file 5 RVs (i.e. data from the literature. *Bottom:* A phase plot of all our new file 6 to file 9 RVs. SPEFO Hα and Hδ RVs were used for the new spg. 6 to 9 spectra. Small dots denote the $O-C$ residuals from the orbital solution. All RVs in the two lower panels were corrected for the difference in γ velocities, adopting γ of the most numerous file 9 as the reference. In all plots, the orbital period of $25\overset{\mathrm{d}}{.}41569$ and the reference epoch of the periastron passge RJD = 43838.5 from the first solution of Table 4 were used. The rms errors of individual RVs are shown whenever available.

Only observations by Abt (1970) and our new RVs are numerous enough to identify the true orbital period. Their periodograms are mutually similar. One can see the dominant period of $25\overset{\mathrm{d}}{.}416$ (f = 0.0393 c d^{-1}) and its first harmonics. A smaller minimum at 0.0360 c d^{-1} corresponds to a 1 yr alias of the $25\overset{\mathrm{d}}{.}416$ period.

3.2. Trial orbital solutions

To investigate the RV variations in a quantitative way, we derived some trial orbital solutions with the program FOTEL (Hadrava

Table 4. Exploratory FOTEL orbital solutions for RVs from the literature and from our red spectra.

Element	Files 2 – 8	Gauss He I	SPEFO He I
P (d)	25.41569(42)	25.41569 fix.	25.41569 fix.
$T_{\rm periastr.}$	43838.5(1.0)	54386.63(80)	54385.16(84)
$T_{\rm super.c.}$	43836.1	54384.28	54383.92
$T_{\rm RVmax.}$	43829.9	54378.04	54378.33
e	0.104(23)	0.181(31)	0.162(28)
ω (°)	131(15)	137(12)	115(12)
K_1 (km s^{-1})	24.0(1.2)	38.0(1.7)	41.6(1.5)
γ_2 (km s^{-1})	−29.3(4.8)	–	–
γ_3 (km s^{-1})	−15.9(1.7)	–	–
γ_4 (km s^{-1})	−16.5(1.2)	–	–
γ_5 (km s^{-1})	−8.4(1.0)	–	–
γ_6 (km s^{-1})	−16.4(1.1)	−6.0(1.8)	−15.0(1.7)
γ_7 (km s^{-1})	−8.4(1.3)	−9.5(1.5)	−10.8(4.7)
γ_8 (km s^{-1})	−12.1(1.3)	−6.1(1.9)	−9.1(2.1)
γ_9 (km s^{-1})	−12.35(0.75)	−12.9(1.3)	−13.7(1.3)
rms (km s^{-1})	4.45	7.03	7.41
No. of RVs	131	72	72

Notes. All epochs are in RJD; rms is the rms of 1 observation of unit weight. **Error of epoch is smaller if one uses a reference epoch close to the centre of the interval covered by data. For an easier comparison of the first solution with the remaining two we also provide corresponding recalculated epochs: RJD 54386.0, RJD 54383.6, and RJD 54377.4 .**

1990, 2004a). We first calculated an orbital solution based on our new SPEFO RVs. It turned out that the semiamplitude for the He I 6678 Å RVs is higher than that obtained from the Hα RVs. This is a well-known effect for early-type stars that the lines with appreciably Stark-broadened wings like the Balmer lines give lower RV amplitudes and are not suitable for the determination of true orbital elements (e.g. Andersen 1975; Andersen et al. 1983). This clearly represents another complication on the way to obtaining realistic binary properties.

Since our first task is, however, to derive the correct value of the orbital period, we adopted the SPEFO Hα RVs and Hδ RVs for the Aurelie spectra, which give a semiamplitude closer to those found by previous investigators – cf. Tab. 1. We combined them with all RVs from the literature and run a solution, in which we allowed calculation of individual systemic velocities (γ's) for individual datasets. Using the rms errors of individual sets, we derived their weights inversely proportional to the squares of the corresponding rms errors. Investigating the phase plots, we found that RVs of spectrograph 1 (Mt. Wilson) refer probably to a combination of the broad and narrow parts of the line profiles and cannot contribute meaningfully to constrain the orbital period – see the top panel of Fig. 4.

We therefore restricted our period analyses only to weighted RVs of spectrographs 2 to 9. Splitting the data into two slightly overlapping subsets, RJD 24010 – 53026, and RJD 50967 – 57329, we derived two trial solutions to check on possible secular changes. **We obtained**

$P = 25\overset{\rm d}{.}$**41710(94),** $e = 0.131(45)$**, and** $\omega = 165(18)°$**,**
and
$P = 25\overset{\rm d}{.}$**4127(12),** $e = 0.132(25)$**, and** $\omega = 137(12)°$

for the first and second subset, respectively. For the time being, there is no compelling evidence for either a period change or a slow apsidal advance within the limits of respective errors.

We then calculated a joint solution for all weighted RVs from files 2 – 8 (see the first solution in Tab. 4) and **we shall adopt the orbital period from this solution,** $P = 25\overset{\rm d}{.}41569 \pm 0\overset{\rm d}{.}00042$**, throughout the rest of this paper. Phase plots for this joint solution are shown in Fig. 4, separately for the RVs from the literature and for our new Hα and Hδ RVs.**

Keeping the orbital period fixed, we then derived two other solutions, this time based on our new He I 6678 Å RVs from files 6 – 9 and using alternatively the RV set based on the Gaussian fits, and on the SPEFO RVs. The results are also in Tab. 4. The elements show that it is not easy at the present stage of research to choose the correct values of K_1 and the mass function. The semi-amplitude and eccentricity differ for the individual solutions, depending on the line(s) measured and also on the measuring technique. A part of the problem is also the fact that almost all spectral lines are to some extent affected by neighbouring blends. To obtain a more realistic estimate of the true orbital elements of the $25\overset{\rm d}{.}4$ orbit, we used SPEFO RVs of all stronger metallic lines in the blue, yellow and red parts of the spectra and derived another orbital solution, allowing for individual 'systemic' velocities for RVs from each ion to eliminate the effects of the line blending. **This exploratory solution indeed confirmed a higher semi-amplitude of 40.1(2.1) km s^{-1} and very pronounced effects of the line blending on the individual RV zero points (a range from** −39.6(2.1) **km s^{-1} for the He I 4472 Å line to** +16.8(2.7) **km s^{-1} for the He I 5016 Å line).**

As further discussed in sect. 4, a substantial part of the problem lies in the fact that the instantaneous shape of the line profiles is also affected by the rapid physical changes, first detected from photometry. Since the broad-line star is rapidly rotating, one can expect from analogy with other known line-profile variables (like their prototype ζ Oph: Walker et al. 1979) that the profile disturbances travel from one wing of the profiles to another brought by rotation. One can conjecture that the RV measurements in SPEFO, i.e. setting on the outer wings of the line profiles, will be more sensitive to such disturbances than when one measures RVs with the help of two Gaussians. We therefore measured RVs of all other spectral lines in the blue and yellow parts of the Aurelie, Elodie and Bernard Lyot spectra with SPEFO. Also the rms errors are quite large: **For instance, the rms errors of a vast majority of He I 6678 Å RVs from the repeated measurements is below 2 km s^{-1} (see Table A.2), which is much smaller than the RV deviations from the orbital RV curves.** That is why we consider the large scatter around the orbital RV curves to be another indirect indication of the disturbance of these RVs by *physical changes of the line profiles*.

Concerning the visual 62000 d orbit, it is true that the systemic velocities from the first solution of Tab. 4 seem to indicate some secular trend with time. However, their heterogeneity and the fact that the semi-amplitudes of RV curves for different stellar lines differ, and the systemic velocities depend on the lines measured due to blends prevent us from using the systemic velocities to constrain the motion in the long orbit. Only continuing observations and analyses based on the same, unblended spectral lines could help in this respect in the future.

Table 5. Parameters of the primary and tertiary derived from a comparison of **selected wavelength segments of the observed** and interpolated synthetic spectra of the primary and tertiary.

Element	Primary	Tertiary
$T_{\rm eff}$ (K)	15850(400)	14920(490)
log g [cgs]	3.68(12)	3.80(15)
$L_{4000-4280}$	0.709(54)	0.295(54)
$L_{4308-4490}$	0.700(48)	0.302(48)
$L_{4700-5025}$	0.701(65)	0.305(64)
$L_{6670-6690}$	0.704(60)	0.295(60)
$v \sin i$ (km s^{-1})	179(6)	72(4)

3.3. RVs measured with the help of synthetic spectra

We tried to disentangle the lines of the system components using the KOREL program (Hadrava 1995, 1997, 2004b). However, since the spectra at our disposal cover only one tenth of the visual orbit for the He I 4143 Å line, and even less for the other spectral lines, the semi-amplitudes of the bodies in the outer orbit could not be meaningfully converged and one has, a priori, no firm clue how to fix them. We only verified that no trace of the secondary could be found. This in our experience implies that the secondary must be for more than 3 mags. fainter than the combined light of the primary and tertiary.

To overcome the problem of severe line blending, we used the Python program PYTERPOL, which interpolates in a precalculated grid of synthetic spectra. Using a set of observed spectra it tries to find the optimal fit between the observed and interpolated model spectra with the help of a simplex minimization technique. It returns the radiative properties of the system components such as $T_{\rm eff}$, $v \sin i$, or log g , but also the relative luminosities of the system components and RVs of individual spectra.[1] The function of the program is described in detail in Nemravová et al. (2016).

In our particular application, two grids of synthetic spectra, Lanz & Hubeny (2007) for $T_{\rm eff}$>15000 K, and Palacios et al. (2010) for $T_{\rm eff}$ <15000 K, were used to estimate basic properties of the primary and tertiary and to derive RVs of all 16 Aurelie, 3 Elodie and 13 Bernard Lyot high-S/N spectra. The following spectral regions containing numerous spectral lines but avoiding the inter-order transitions and regions with stronger telluric lines were modelled simultaneously:

4000–4025 Å, 4097–4155 Å, 4260–4280 Å,
4308–4405 Å, 4450–4490 Å, 4700–4725 Å,
4817–4935 Å, 5008–5025 Å, and 6670–6690 Å.

Relative component luminosities were fitted separately in four spectral bands: 4000–4280 Å, 4308–4490 Å, 4700-5025 Å, and 6670–6690 Å.

Uncertainties of kinematic and radiative properties were obtained through Markov chain Monte Carlo (MCMC) simulation implemented within emcee[2] Python library by Foreman-Mackey et al. (2013). They are summarised in Tab. 5. The individual RVs are listed in Table A.4.

[1] The program PYTERPOL is available with a tutorial at *https://github.com/chrysante87/pyterpol/wiki* .

[2] The library is available through GitHub https://github.com/dfm/emcee.git and its thorough description is at http://dan.iel.fm/emcee/current/.

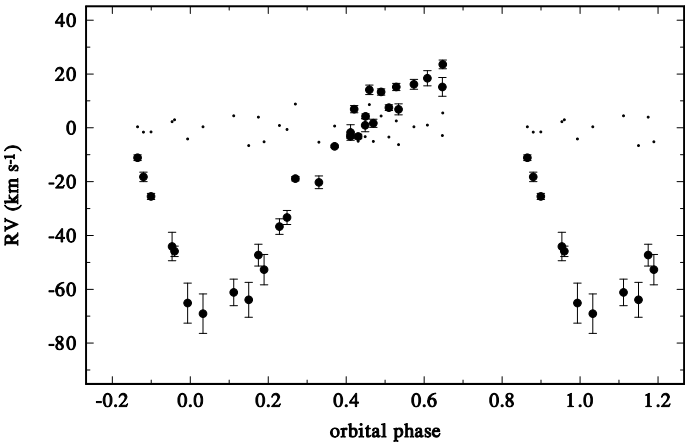

Fig. 5. Final RV curve of V746 Cas based on RVs derived with the help of the program PYTERPOL. Small dots denote the $O-C$ deviations of individual RVs from the orbital solution.

Table 6. Final FOTEL orbital solution for RVs from high-resolution spectra derived with the help of the program PYTERPOL.

Element	Value with error
P (d)	25.41569 fixed
$T_{\rm periastr.}$	54387.05(44)
$T_{\rm super.c.}$	54384.65
$T_{\rm RVmax.}$	54378.17
e	0.249(26)
ω (deg.)	145.0(7.3)
K_1 (km s^{-1})	44.5(1.4)
γ (km s^{-1})	−17.37(85)
$f(M)$ ($M_\odot$)	0.2113
rms (km s^{-1})	4.15
No. of RVs	32

Notes. All epochs are in RJD; rms is the rms of 1 observation of unit weight.

3.4. Final orbital solution

Using the RVs derived with the help of PYTERPOL (their errors estimated from the MCMC simulation being a few km s^{-1}), we derive the final orbital solution to be used to estimate the properties of the inner binary system. This solution is in Tab. 6 and the corresponding RV curve is shown in Fig. 5. It is reassuring to note that when we allowed for a free convergence of the orbital period, we arrived at a value of $25^{\rm d}.4156(13)$, which agrees **with the value adopted here. We therefore recommend to adopt the linear ephemeris**

$$T_{\rm super.conj.} = \text{HJD } 2454384.65(44) + 25^{\rm d}.41569(42) \quad (1)$$

as currently the best one.

4. The spectral signatures and nature of rapid variations

4.1. Overview and analysis of previous results

Table 7 provides an overview of various frequencies of light variations of V746 Cas reported by several investigators. There

Table 7. Frequencies and periods of light variations of V746 Cas found by various investigators.

Frequency ($c\,d^{-1}$)	Period (d)	Source	Identification
0.94	1.06	1	f_1
0.939	1.06	2	f_1
0.399	2.51	2	f_2
0.93914(3)	1.06480	3	f_1
0.39934(4)	2.50413	3	f_2
0.39923(4)	2.50413	4	f_2
0.93895(4)	1.06502	4	f_1
0.79906(9)	1.25147	4	$2f_2$
0.96630(9)	1.03488	4	
0.39946(4)	2.50338	5	f_2
0.93895(4)	1.06502	5	f_1
1.20346(6)	0.830937	5	$3f_1$?
0.9390	1.065	6	f_1
0.3994	2.504	6	f_2
0.9309	1.074	6	
0.7988	1.252	6	$2f_2$

Notes. *Column "Source":* 1...Waelkens et al. (1998), H_p photometry; 2...Andrews & Dukes (2000), Four College APT and H_p photometry; 3...Mathias et al. (2001), H_p photometry; 4...De Cat et al. (2004), Geneva 7C and H_p photometry; 5...De Cat et al. (2007), Geneva 7C photometry; 6...Dukes et al. (2009), Four College APT, Geneva 7C and H_p photometry.

seems to be no doubt about the presence of two principal frequencies, detected by all investigators, 0.939 and 0.399 $c\,d^{-1}$. Notably, Mathias et al. (2001) were unable to find any spectroscopic signatures of these two frequencies in their Aurelie spectra covering the wavelength interval from 4085 to 4155 Å. The authors admit, however, that all their spectra have S/N's lower than 140. Two groups, De Cat et al. (2004) and Dukes et al. (2009) reported another frequency, 0.799 $c\,d^{-1}$. De Cat et al. (2004) denoted it as a possible alias. We note that it is actually an exact harmonics of the 0.399 $c\,d^{-1}$ frequency. This, in our opinion simply indicates that the light curve with the 0.399 $c\,d^{-1}$ frequency deviates from a sinusoidal shape. Therefore, the 0.799 $c\,d^{-1}$ frequency is *not* an independent frequency. Another weak frequency of 1.20346 $c\,d^{-1}$ reported by De Cat et al. (2007) (which in our opinion could be the second harmonics of 0.399 $c\,d^{-1}$) could not be confirmed by Dukes et al. (2009), who analysed their own Strömgen *uvby* photometry from the Four College Automatic Photoelectric telescope (APT) along with the H_p and Geneva 7-C photometries. They found, however, a frequency of 0.9309 $c\,d^{-1}$, quite close to $f_1 = 0.939$ $c\,d^{-1}$. We note that the 0.9390 and 0.9309 $c\,d^{-1}$ mutually differ for 1/3 of the frequency of a sidereal year, so we suspect that the 0.9309 cd^{-1} frequency is an alias. The above facts led us to suspect that the light changes of V746 Cas are modulated *only by two independent periods*.

4.2. New period analysis of available photometry

For the purpose of the period analysis, we subtracted seasonal mean values from all data to remove possible slight secular variations of either instrumental systems of the telescopes or true small secular changes (see Appendix C for details). We used the programs `PERIOD04` (Lenz & Breger 2005) and `FOTEL` for the modelling and fits. We found that the longer, non-sinusoidal period of 2.5 d has larger amplitudes also for the second and fifth harmonics (periods $1^d.25194$, and $0^d.50077$), which were then included into fits. Inspecting cases with more observations within short time intervals like 0.03 d, we conclude that in all three data sets there are cases when the rms error of single observations exceed $0^m.007$. The rms error of the fit is only slowly decreasing when one adds more frequencies and remains on the $0^m.007$ level.

We arrive at the following ephemerides for the $1^d.065$, and $2^d.504$ periods:

$$T_{\rm max.light} = {\rm RJD}\ 52540.2866(61) + 1^d.0649524(40) \quad (2)$$

$$T_{\rm max.light} = {\rm RJD}\ 52242.585(32) + 2^d.503867(19). \quad (3)$$

4.3. Periodic variations of the magnetic field

We tried to see whether the observed variations of the magnetic field found by Neiner et al. (2014) could not be related to the known photometric changes. We quickly found that the magnetic field indeed varies with the longer of the photometric periods, $2^d.50387$ – see Fig. 6.

It is usual that a sinusoidal variation of the intensity of magnetic field is interpreted as a dipole field inclined to the rotational axis of the star and varying with the stellar rotational period. Neiner et al. (2014) associated the magnetic field with the narrow lined component, which they considered to be the primary but which is – as we have shown here – the distant tertiary component moving in the long orbit with the $25^d.4$ binary.

4.4. Rapid line-profile changes?

We inspected the $O-C$ RV residuals from the $25^d.4$ orbit for the `SPEFO` He I 6678 Å RVs. We used the `SPEFO` RVs based on repeated settings on the outer line wings, which are presumably more sensitive to the profile disturbances than the RVs based on the fits of the Gaussian profiles. In Fig. 7 we compare the plot of these RV residuals with the plot of yellow photometry prewhitened for the $2^d.50387$ period. There is some indication of phase changes with the photometric period of $1^d.065$ but the scatter around the mean curve is uncomfortably large and the result certainly needs verification with the help of whole-night series of high-S/N spectra. However, in our opinion, there is a reason to identify the $1^d.065$ period with the rotational period of the primary. The modulation of measured RVs could be caused by some structures on the surface of the primary, moving across the stellar disk as the star rotates. We note that there is growing evidence for rotational modulation for a number of B stars from the photometry obtained by the Kepler satellite and by ground-based surveys (see, e.g. McNamara et al. 2012; Nielsen et al. 2013; Kourniotis et al. 2014; Balona et al. 2015; Balona 2016).

We also tried to detect the line-profile changes in the residuals from `PYTERPOL` solution for high-S/N spectra. It must be kept in mind that all these spectra available to us were obtained with a frequency of one spectrum per night and their number is

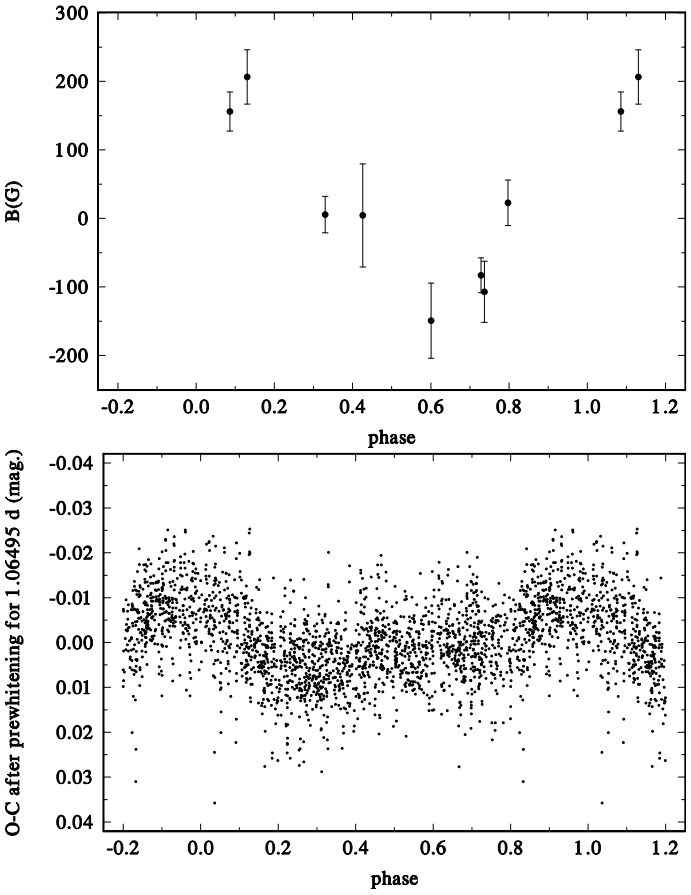

Fig. 6. *Top panel:* A phase plot of the magnetic field observations from measurements of Neiner et al. (2014) from spectra not affected by technical problems and for the mean values from all lines. The rms errors of measurements are shown by error bars. *Bottom panel:* A phase plot of all yellow photometric observations prewhitened for the $1^{\rm d}06495$ period. In both panels, the data are plotted vs. phase of the $2^{\rm d}.503867$ period given by ephemeris 3.

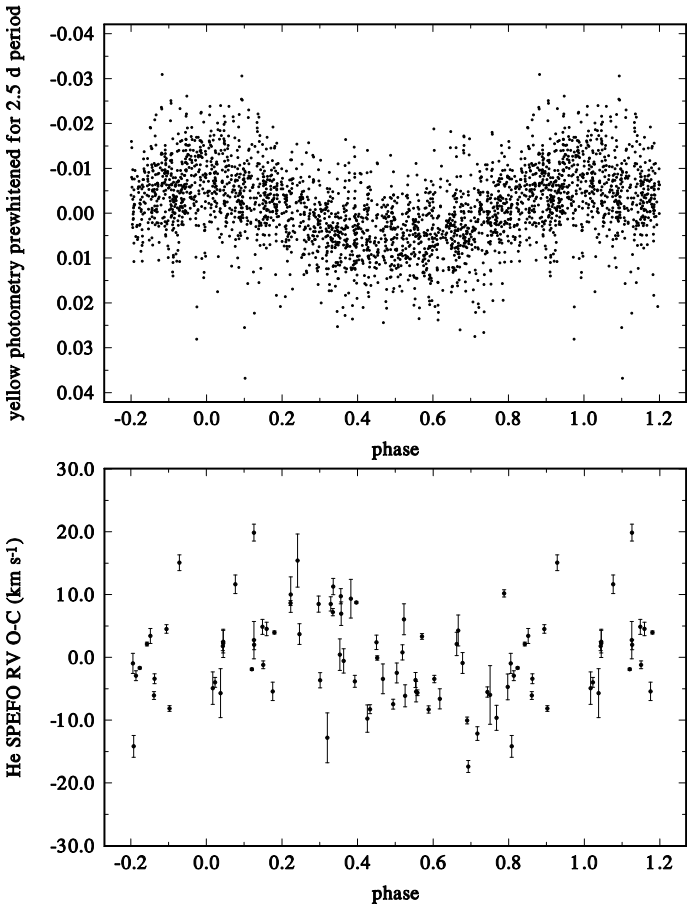

Fig. 7. Phase plots for the $1^{\rm d}06495$ period calculated using ephemeris 2. ***Top:*** **All yellow photometry $O-C$ residuals prewhitened for the 2.5 d period and its harmonics.** ***Bottom:*** **A plot of the residuals from the orbital solution for the SPEFO He I 6678 Å RVs for the subsets of Aurelie and Bernard Lyot spectra.**

low. We show an example of dynamical spectra for the 4450 – 4490 Å region plotted vs. phase of the $1^{\rm d}.065$ period. Some sinusoidal variation in the wings of He I 4472 Å, Mg II 4481 Å, and several weaker lines can be suspected but we admit that with the spectra at hand, the evidence is not compelling.

5. Towards a model of the system

We have demonstrated that V746 Cas is a challenging triple system with a broad-lined B-type primary, a low-mass secondary (as yet undetected in the optical spectra) and a tertiary, known already from visual and speckle-interferometric observations. Our dynamical spectra (cf. Fig. 2) as well as the line profiles of the He I 4713 Å shown by Neiner et al. (2014) demonstrate that the tertiary must also be of spectral type B. Obvious presence of rapid light and line-profile variations and the absence of the spectral lines of the secondary in the optical spectra prevents us from a *direct* determination of all component masses and radii, however, some of the system properties can be estimated from already known facts and a consistent picture of the system can be obtained.

5.1. Properties of the close $25^{\rm d}.4$ binary

The facts, which must be taken into account are as follows:

- All available MKK spectral classifications of V746 Cas summarized in the SIMBAD bibliography, including a recent one by Tamazian et al. (2006) based on high-resolution spectra, agree on the spectral type B5 IV. Dereddening of the mean all-sky standard *UBV* magnitudes from Hvar (see Tab. C.1) gives $V_0 = 5\overset{\rm m}{.}43$, $(B-V)_0 = -0\overset{\rm m}{.}170$, $(U-B)_0 = -0\overset{\rm m}{.}635$, and $\mathrm{E}(B-V) = 0\overset{\rm m}{.}055$, which corresponds to a B4-5IV star after the calibration by Golay (1974).
- We calculated evolutionary tracks for the system components using the Mesastar program (Paxton et al. 2015) and compared them with the observed range of the values of $T_{\rm eff}$ and $\log g$, deduced from the line-profile fits, in Fig. 9. From this comparison one can estimate the mass of the primary to be $M_1 = 6.2\,\mathrm{M}_\odot$ (range from 5.6 to 6.7).
  We verified that the evolutionary tracks in the considered region close to the terminal main sequence (TAMS) *are not sensitive* to the value of metallicity (we checked tracks for $Z = 0.04$), or the mixing-length parameter α (for instance, $\alpha = 1.6$ leads to essentially the same results) since both stars are in a radiative equilibrium.
- One can safely exclude the presence of binary eclipses from available photometry (see Fig. 10). Our simulations of the light curve for the $25^{\rm d}.4$ orbit with the program PHOEBE 1

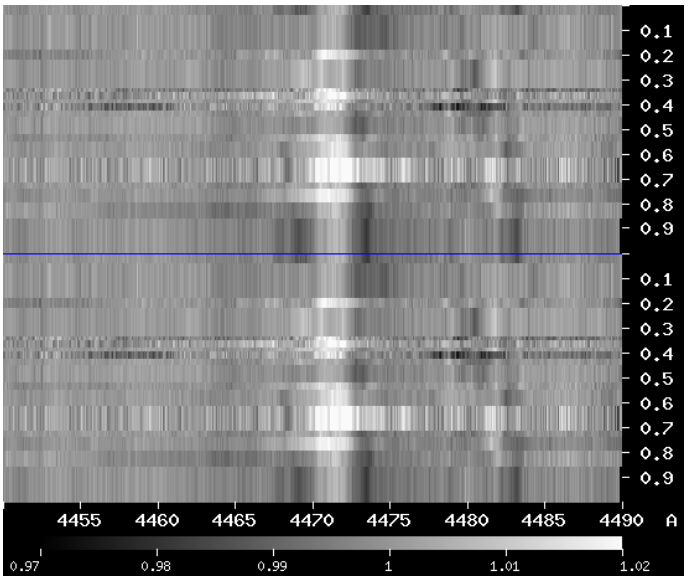

Fig. 8. Dynamical spectra of the residuals from the PYTERPOL solution in the region of He I 4472 and Mg II 4481 Å lines plotted vs. phase of the 1.d065 period using ephemeris (2)

Table 8. Range of masses M_2 of the unseen secondary component of V746 Cas estimated from the mass function $f(M)$ of Tab. 6, and a plausible range of the primary star mass M_1, according to Fig. 9, for a range of inclinations i of the 25.d416 orbit. The case $i = 50°$ seems already excluded, because the resulting M_2 value is too large with respect to Fig. 11.

	$M_1 = 5.6$ M$_\odot$		$M_1 = 6.2$ M$_\odot$		$M_1 = 6.5$ M$_\odot$	
i (°)	M_2 (M$_\odot$)	M_2/M_1	M_2 (M$_\odot$)	M_2/M_1	M_2 (M$_\odot$)	M_2/M_1
85.0	2.39	0.427	2.54	0.409	2.61	0.401
80.0	2.42	0.433	2.57	0.415	2.64	0.407
70.0	2.57	0.459	2.73	0.440	2.80	0.431
64.0	2.72	0.486	2.89	0.465	2.97	0.456
50.0	3.35	0.599	3.55	0.572	3.64	0.560

(Prša & Zwitter 2005) for plausible values of the stellar radii (see below) then show there is a rather strict *upper* limit for the orbital inclination, $i < 85°$.

– The final orbital solution for all PYTERPOL RVs from Tab. 6 gives the mass function $f(M) = 0.2113$ M$_\odot$. Using this value and the plausible range of the primary mass, one can estimate possible secondary masses for different orbital inclinations (see Tab. 8).

We can also use the observed Hipparcos parallax p of V746 Cas to further constrain possible properties of the system. According to the improved reduction (van Leeuwen 2007a,b) $p = 0.''00326(63)$. Assuming the above mentioned $V_0 = 5.^m43$ for the whole system, the observed magnitude difference between the primary and tertiary and neglecting the light contribution from the unseen secondary, one arrives at $V_0^1 = 5.^m82$ for the primary. Using the above-mentioned range of the possible values of the parallax, 0.″00263 to 0.″00394 one obtains $M_V^1 = -2.^m08$ and $-1.^m20$, respectively. The bolometric corrections for the considered range of the effective temperature of

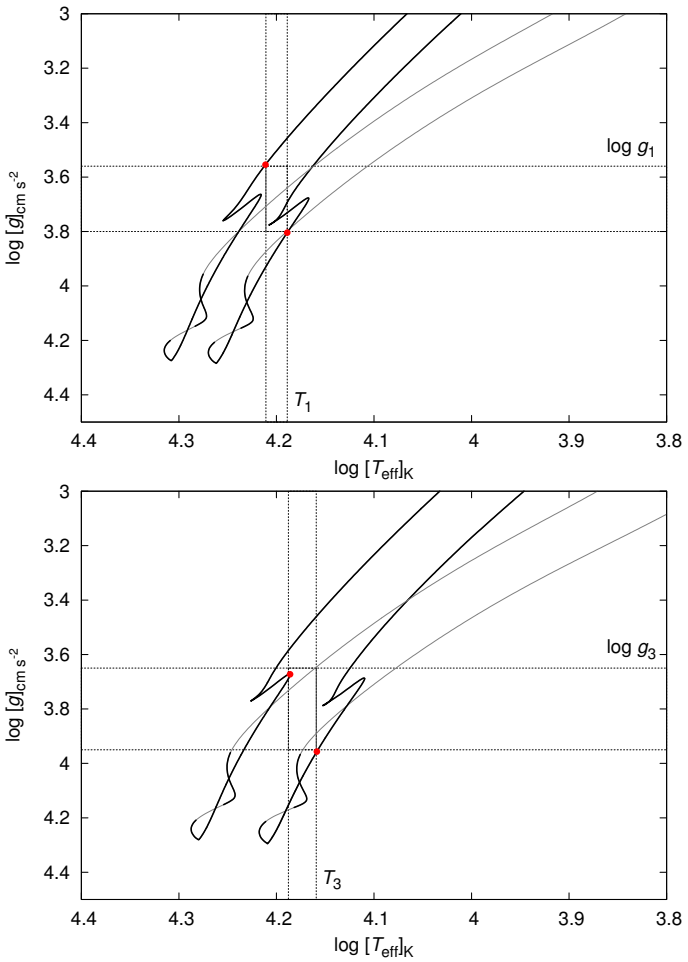

Fig. 9. Evolutionary tracks in effective temperature $T_{\rm eff}$ vs surface gravity $\log g$ plots, including pre-MS (thin line), MS and SGB phases (thick line). Top panel shows the primary component of V746 Cas, with the nominal value of mass $M_1 \doteq 6.2\,M_\odot$ and range $5.6\,M_\odot$ to $6.7\,M_\odot$. The corresponding times (counted from pre-MS) to reach the uncertainty intervals are 56 Myr and 43.7 Myr, respectively. If we would account for pre-MS tracks too, the range would be even larger. Bottom panel shows the tetriary, with $M_2 = 5.3\,M_\odot$ and range $4.6\,M_\odot$ to $6.0\,M_\odot$; the times are 73 Myr and 54 Myr. In all cases we assumed the helium abundance $Y = 0.274$, metallicity $Z = 0.0195$, mixing length parameter $\alpha = 2.1$, We also accounted element diffusion, Reimers RGB wind with $\eta = 0.6$, Blocker AGB wind with $\eta = 0.1$, even though neither is very relevant on ZAMS. The maximum output time step was $\Delta t = 10^5$ yr to resolve TAMS. Mesastar program, rev. 8845 (Paxton et al. 2015) was used for these computations.

the primary are from $-1.^m433$ to $-1.^m557$ so that the extreme allowed values of the bolometric magnitude of the primary $M_{\rm bol}^1$ are $-2.^m63$ to $-3.^m64$.

Fig. 11 shows that this range for $M_{\rm bol}^1$ further restricts the plausible range of primary mass $M_1 = 5.6$ to $6.5\,$M$_\odot$. Moreover, according to synthetic spectra (Figs. B.1 to B.3) there is an upper limit for the relative flux of the unseen secondary component, about 0.02, which corresponds to the magnitude difference of 4.2 mag. Consequently, there has to be a *lower* limit for the orbital inclination of the 25.d4 orbit, about $i > 70°$ according to Tab. 8, otherwise M_2 would be too high and its spectral lines should be definitely observable. The secondary thus should be an A star. Our estimates predict the semi-amplitude of the RV curve of the secondary in the range of about 100 to 110 km s^{-1}.

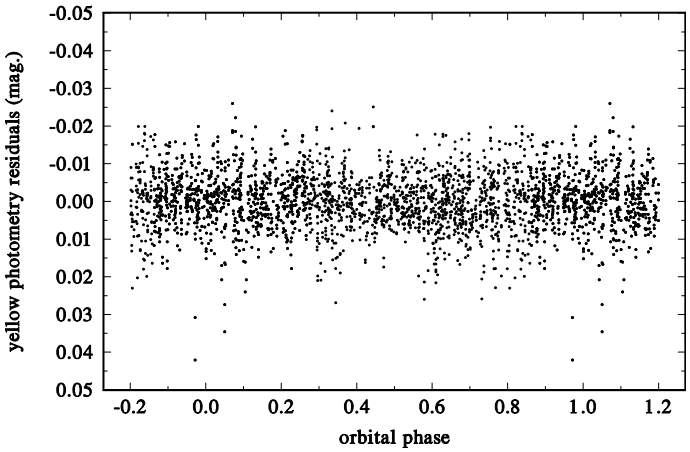

Fig. 10. All yellow photometric observations prewhitened for both the $1^{\rm d}.065$ period, and the $2^{\rm d}.5039$ period and its harmonics, plotted vs. orbital phase from ephemeris (1).

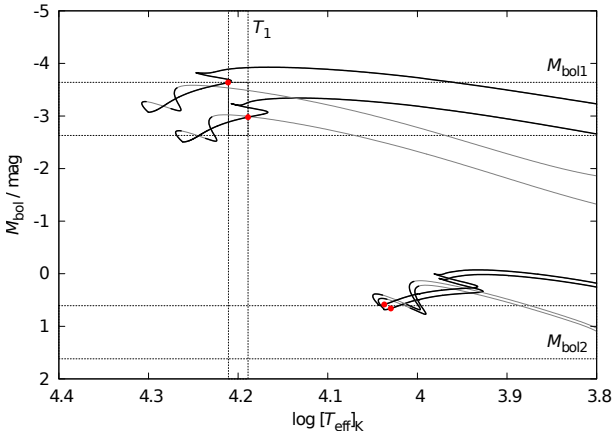

Fig. 11. The Hertzsprung–Russel diagram for the primary (top) and secondary (bottom) components of V746 Cas . These tracks correspond to the following ranges of masses: $M_1 = 6.5\,M_\odot$ to $5.6\,M_\odot$, and $M_2 = 2.55\,M_\odot$ to $2.60\,M_\odot$. The times to reach the uncertainty intervals (56 to 44 Myr) are the same for both stars. The upper limit of M_1 is slightly lower than in Fig. 9 in order to match the upper limit of the bolometric magnitude $M^1_{\rm bol}$ inferred from Hipparcos parallax. The lower limit of M_2 is given by the mass function $f(M)$ of the close binary and no-eclipses condition. Finally, the upper limit of M_2 is estimated from the maximum relative flux of the unseen component (about 0.02; cf. Figs. B.1 to B.3), which corresponds to the magnitude difference of 4.2 mag. Other parameters of the stellar evolution model are the same as in Fig. 9.

Should $1^{\rm d}.065$ be the rotational period of the primary, then for $v \sin i = 179$ km s^{-1}, derived from the PYTERPOL solution for the primary, $R_1 \geq 2\pi\, v \sin i/P = 3.77\,{\rm R}_\odot$. For instance, if $i = 70°$ one gets $R_1 = 4.01\,{\rm R}_\odot$. For the expected range of the primary mass this would imply log $g = 3.98$ to 4.04 [cgs] for the primary which is slightly offset at the 2.5-σ level with respect the range deduced from the fit by synthetic spectra (Tab. 5). On the other hand, should the true rotational period be a photometric double-wave curve with a period twice longer, i.e. $2^{\rm d}.130$, one would obtain log $g = 3.38$ to 3.44 [cgs]; again offset from the nominal range. This would also correspond to significantly larger radius $R_1 = 8.02\,{\rm R}_\odot$ and even lower upper limit of i. Given all the uncertainties involved, however, one should still keep both possibilities in mind in future dedicated studies.

5.2. Tetriary component

Regarding the tetriary component, the analysis of the $T_{\rm eff}$ vs log g plot led to the mass $M_3 = 5.3\,{\rm M}_\odot$ (range from 4.6 to 6.0; Fig. 9). Within the uncertainties, the primary and tetriary stars can even be equally massive and have very similar effective temperatures. The similarity of the primary and tertiary is also supported by the fact that their relative luminosities over the whole optical range seem to be the same — see Tab. 5.

The more recent estimates of the magnitude difference between the close binary and tertiary from astrometry (Perryman & ESA 1997; Mason et al. 2009) agree on $m_{3\,\rm V} - m_{(1+2)\,\rm V} \sim 0^{\rm m}.9$. The relative luminosities of the primary and tertiary estimated with PYTERPOL (see Tab. 5) imply $m_{3\,\rm V} - m_{(1+2)\,\rm V} = 0^{\rm m}.92$, in a remarkable agreement with the astrometric estimates. This once more confirms our identification of the narrow-line component seen in the spectra with the tertiary.

Using the $v \sin i = 72$ km s^{-1} estimated from the PYTERPOL solution for the tertiary and adopting the $2^{\rm d}.504$ period as its period of rotation, we can similarly estimate the radius of the tertiary $R_3 \geq 3.56\,{\rm R}_\odot$. Assuming that the inclination of the rotational axis of the tertiary is identical with the orbital inclination of the outer orbit 64°, one estimates log g from 3.90 to 4.01 for it. This agrees quite well with the observed range of log g from the line-profile modelling.

6. Conclusions

Our main findings can be finally summarised:

1. The rapidly rotating B4-B5 primary moves in the orbit with an unseen secondary with a semi-amplitude of ~ 47 km s^{-1}, the more accurate determination being hampered by the probable presence of line profile variations with the dominant photometric period of $1^{\rm d}.065$.
2. The fact that the secondary could not be detected in the optical spectra, even when using the spectra disentangling, and the observed mass function imply that it should be an A star.
3. The bipolar magnetic field, discovered by Neiner et al. (2014), varies with the photometric period of $2^{\rm d}.50387$. It is associated with the tertiary, which is in a wide orbit with the $25^{\rm d}.4$ binary. The tertiary is a ~B5-6IV star, which contributes 30 % of the light in the optical region.
4. The photometric periods $1^{\rm d}.065$ and $2^{\rm d}.504$ are tentatively identified with the rotational periods of the primary and tertiary, respectively. However, the identification of the former period needs a verification by future dedicated studies.
5. Very accurate systematic photometric observations relative to some truly constant comparison star and new spectral observations consisting of whole-night series are needed to progress in the understanding of this system.
6. Attempts to detect faint spectral lines of the unseen secondary should probably be conducted in far-IR region.
7. The classification of V746 Cas as an SPB variable should be critically re-examined.

Acknowledgements. We profited from the use of 13 echelle spectra from the Bernard Lyot telescope, made publicly available via the Polar Base web service and Geneva 7-C photometry made available via HELAS service, to which we were kindly directed by Dr. C. Aerts. Dr. P. Mathias kindly provided us with old archival DAT tapes with the original Aurelie spectra of ten B stars and some advice about their content and structure. The spectra were reconstructed from the tapes with the help of Mr. R. Veselý. Dr. H. Božić, Ms. K. Hoňková and Mr. D. Vršnjak kindly obtained some of the calibrated *UBV* observations of V746 Cas and its comparison stars for us. We acknowledge the use of the public versions of programs FOTEL and KOREL, written by Dr. P. Hadrava and PHOEBE 1.0 written by Dr. A.Prša. The research of PH, PM, and JN was supported by

the grant P209/10/0715 of the Czech Science Foundation. JN and PH were also supported by the grants GA15-02112S of the Czech Science Foundation and No. 250015 of the Grant Agency of the Charles University in Prague. Research of DK was supported by a grant GA17-00871S of the Czech Science Foundation. Our thanks are due to Dr. M. Wolf, who obtained one Ondřejov spectrum used here and who provided a few useful comments to this paper. We also appreciate constructive criticism by an anonymous referee, who helped us to re-think the whole study an to present our arguments and analyses in a better way. The use of the NASA/ADS bibliographical service and SIMBAD electronic database are gratefully acknowledged.

References

Abt, H. A. 1970, ApJS, 19, 387
Abt, H. A., Gomez, A. E., & Levy, S. G. 1990, ApJS, 74, 551
Adams, W. S. 1912, ApJ, 35, 163
Andersen, J. 1975, A&A, 44, 445
Andersen, J., Clausen, J. V., Gimenéz, A., & Nordström, B. 1983, A&A, 128, 17
Andrews, K. E. & Dukes, R. J. 2000, in Bulletin of the American Astronomical Society, Vol. 32, American Astronomical Society Meeting Abstracts, 1477
Balona, L. A. 2016, MNRAS, 457, 3724
Balona, L. A., Baran, A. S., Daszyńska-Daszkiewicz, J., & De Cat, P. 2015, MNRAS, 451, 1445
Blaauw, A. & van Albada, T. S. 1963, ApJ, 137, 791
Chini, R., Hoffmeister, V. H., Nasseri, A., Stahl, O., & Zinnecker, H. 2012, MNRAS, 424, 1925
De Cat, P., Briquet, M., Aerts, C., et al. 2007, A&A, 463, 243
De Cat, P., De Ridder, J., Uytterhoeven, K., et al. 2004, in Astronomical Society of the Pacific Conference Series, Vol. 310, IAU Colloq. 193: Variable Stars in the Local Group, ed. D. W. Kurtz & K. R. Pollard, 238
de Mink, S. E., Langer, N., Izzard, R. G., Sana, H., & de Koter, A. 2013, ApJ, 764, 166
Doboco, J. A. & Ling, J. F. 2005, IAU Com. 26 Inf. Circ. No., 156, 1
Dukes, R. J., Bramlett, J., & Sims, M. 2009, in American Institute of Physics Conference Series, Vol. 1170, American Institute of Physics Conference Series, ed. J. A. Guzik & P. A. Bradley, 379–381
Foreman-Mackey, D., Hogg, D. W., Lang, D., & Goodman, J. 2013, PASP, 125, 306
Gillet, D., Burnage, R., Kohler, D., et al. 1994, A&AS, 108
Golay, M., ed. 1974, Astrophysics and Space Science Library, Vol. 41, Introduction to astronomical photometry
Gómez, A. E. & Abt, H. A. 1982, PASP, 94, 650
Hadrava, P. 1990, Contributions of the Astronomical Observatory Skalnaté Pleso, 20, 23
Hadrava, P. 1995, A&AS, 114, 393
Hadrava, P. 1997, A&AS, 122, 581
Hadrava, P. 2004a, Publ. Astron. Inst. Acad. Sci. Czech Rep., 92, 1
Hadrava, P. 2004b, Publ. Astron. Inst. Acad. Sci. Czech Rep., 92, 15
Harmanec, P. 1998, A&A, 335, 173
Harmanec, P. & Božić, H. 2001, A&A, 369, 1140
Harmanec, P., Horn, J., & Juza, K. 1994, A&AS, 104, 121
Horn, J., Kubát, J., Harmanec, P., et al. 1996, A&A, 309, 521
Hube, D. P. 1970, MmRAS, 72, 233
Hube, D. P. 1983, A&AS, 53, 29
Kourniotis, M., Bonanos, A. Z., Soszyński, I., et al. 2014, A&A, 562, A125
Lanz, T. & Hubeny, I. 2007, ApJS, 169, 83
Lenz, P. & Breger, M. 2005, Communications in Asteroseismology, 146, 53
Mason, B. D., Hartkopf, W. I., Gies, D. R., Henry, T. J., & Helsel, J. W. 2009, AJ, 137, 3358
Mathias, P., Aerts, C., Briquet, M., et al. 2001, A&A, 379, 905
McNamara, B. J., Jackiewicz, J., & McKeever, J. 2012, AJ, 143, 101
McSwain, M. V., Boyajian, T. S., Grundstrom, E. D., & Gies, D. R. 2007, ApJ, 655, 473
Moultaka, J., Ilovaisky, S. A., Prugniel, P., & Soubiran, C. 2004, PASP, 116, 693
Neiner, C., Tkachenko, A., & MiMeS Collaboration. 2014, A&A, 563, L7
Nemravová, J. A., Harmanec, P., Brož, M., et al. 2016, A&A, 594, A55
Nielsen, M. B., Gizon, L., Schunker, H., & Karoff, C. 2013, A&A, 557, L10
Palacios, A., Gebran, M., Josselin, E., et al. 2010, A&A, 516, A13
Palmer, D. R., Walker, E. N., Jones, D. H. P., & Wallis, R. E. 1968, Royal Greenwich Observatory Bulletins, 135, 385
Paxton, B., Marchant, P., Schwab, J., et al. 2015, ApJS, 220, 15
Perryman, M. A. C. & ESA. 1997, The HIPPARCOS and TYCHO catalogues (The Hipparcos and Tycho catalogues. Astrometric and photometric star catalogues derived from the ESA Hipparcos Space Astrometry Mission, Publisher: Noordwijk, Netherlands: ESA Publications Division, 1997, Series: ESA SP Series 1200)
Petit, P., Louge, T., Théado, S., et al. 2014, PASP, 126, 469
Plaskett, J. S. & Pearce, J. A. 1931, Publ. Dom. Astrophys. Obs. Victoria, 5, 1

Table A.3. RVs of the broad wings of the He I 4144 Å line and Hδ of V746 Cas measured in all Aurelie spectra with SPEFO and control measurements of the He I 4144 Å line with the help of Gaussian fits.

RJD	$RV^{He\,I\,4144}_{SPEFO}$	$RV^{H\,\delta}_{SPEFO}$	$RV^{He\,I\,4144}_{Gauss}$
50967.5897	14.96 ± 2.82	−5.86 ± 6.39	3
51005.5778	−39.13 ± 0.69	−19.57 ± 2.05	-36
51006.5970	−49.73 ± 1.20	−33.64 ± 0.19	-44
51007.5940	−48.03 ± 0.57	−43.62 ± 1.82	-54
51009.5946	−52.66 ± 2.46	−45.15 ± 2.56	-49
51010.5765	−60.59 ± 0.57	−42.57 ± 2.72	-41
51011.5748	−52.10 ± 1.75	−31.28 ± 1.02	-32
51012.5773	−42.08 ± 2.36	−29.20 ± 1.76	-24
51036.6214	−46.21 ± 2.26	−38.85 ± 4.98	-37
51038.4965	−35.73 ± 1.60	−26.14 ± 2.35	-33
51040.5680	−24.47 ± 4.67	−17.69 ± 3.08	-13
51042.6335	−13.14 ± 0.55	−11.42 ± 4.79	4
51094.4222	−9.42 ± 3.98	−4.39 ± 4.00	19
51096.5979	15.09 ± 1.94	0.80 ± 3.00	34
51097.5923	28.24 ± 1.28	0.42 ± 3.80	41
51098.4748	25.06 ± 2.97	7.44 ± 4.45	32
51099.4536	26.19 ± 1.81	10.63 ± 2.28	29

Prša, A. & Zwitter, T. 2005, ApJ, 628, 426
Škoda, P. 1996, in ASP Conf. Ser. 101: Astronomical Data Analysis Software and Systems V, 187–189
Stellingwerf, R. F. 1978, ApJ, 224, 953
Tamazian, V. S., Docobo, J. A., Melikian, N. D., & Karapetian, A. A. 2006, PASP, 118, 814
van Leeuwen, F. 2007a, in Astrophysics and Space Science Library, ed. F. van Leeuwen, Vol. 350
van Leeuwen, F. 2007b, A&A, 474, 653
Wade, G. A., Neiner, C., Alecian, E., et al. 2016, MNRAS, 456, 2
Waelkens, C., Aerts, C., Kestens, E., Grenon, M., & Eyer, L. 1998, A&A, 330, 215
Walker, G. A. H., Yang, S., & Fahlman, G. G. 1979, ApJ, 233, 199

Appendix A: Details of the spectral data reduction and measurements

All RVs collected from the astronomical literature are provided in Tab. A.1. Whenever necessary, we derived heliocentric Julian dates (HJDs) for them. RVs derived by us are provided in Tabs. A.2, A.3, and A.4.

Table A.1. Individual RVs of V746 Cas from the astronomical literature. Observing instruments in column "Spg." are identified by the same numbers as in Tab. 2. All RVs are in km s^{-1}.

RJD	RV	Spg.	RJD	RV	Spg.
19026.8885	5.0	1	43461.679	-37.8	4
19027.6501	-35.0	1	43462.790	-21.1	4
19058.7623	.4	1	43508.748	-32.8	4
19382.7240	1.9	1	43726.972	+06.7	4
19409.8989	-1.8	1	43808.852	-05.5	4
22915.9555	-3.7	1	43809.896	-23.4	4
23004.7039	-8.0	1	43810.821	-14.4	4
24010.4054	-5.3	2	43830.758	+03.1	4
24362.4915	5.7	2	43831.648	-02.0	4
24439.1971	-18.0	2	43832.647	-04.2	4
24767.3810	-23.9	2	44068.973	-45.6	4
24777.4394	-51.5	2	44116.922	-27.8	4
24891.1328	-16.7	2	44187.697	+0.4	4
35795.6197	7.0	3	44188.666	+1.9	4
35796.6027	11.0	3	44189.825	-02.0	4
35797.6796	12.0	3	44229.655	-16.0	4
35799.6366	1.0	3	44231.618	-0.8	4
35803.6214	-24.0	3	53657.787	-14.2	5
35804.6644	-24.0	3	53658.833	-4.8	5
35819.5897	-9.0	3	53658.835	-4.3	5
35820.5586	4.0	3	53659.720	-0.3	5
35821.6155	5.0	3	53659.721	-0.1	5
35822.5385	4.0	3	53660.754	3.0	5
35823.5854	4.0	3	53663.735	13.7	5
35824.5884	3.0	3	53685.735	-9.4	5
35830.5580	-12.0	3	53693.635	13.8	5
35831.5949	-16.0	3	53693.790	7.3	5
35832.5589	-34.0	3	53694.701	6.9	5
35833.5528	-40.0	3	53695.674	-1.4	5
43411.860	-36.7	4	53695.769	-0.8	5
43459.731	-42.0	4	53696.565	-4.9	5
43460.730	-44.3	4	53696.789	-2.0	5

Appendix B: Fitting the spectra with interpolated synthetic spectra.

Using the Python program `PYTERPOL` and two grids of synthetic spectra, Lanz & Hubeny (2007) for $T_{\rm eff}$>15000 K, and Palacios et al. (2010) for $T_{\rm eff}$ <15000 K, were estimated the properties of the primary and tertiary, which are summarised in Tab. 5. Figures B.1, B.2, and B.3 show some examples of the comparison of the observed and the best interpolated synthetic spectra in detail, for several different spectrograms and spectral regions.

Appendix C: Details of the photometric data reduction and homogenisation

In an effort to bring at least all yellow photometric observations of V746 Cas on a comparable scale, we used several *UBV* observations of V746 Cas and its comparison stars HR 96 and HD 567 secured with the 0.65 m reflector and photoelectric photometer at Hvar. These observations were reduced to the standard Johnson system with the help of the program HEC22, based on non-linear transformation formulae (Harmanec et al. 1994). Extinction and its variations during observing nights were taken into account during the data reduction.[3] We then used mean all-sky Hvar values of HD 96 and added them to the magnitude differences $y - y_{\rm HR\,96}$ for both, V746 Cas and HD 567 Strömgren APT observations of dataset 12.

Hipparcos $H_{\rm p}$ observations (dataset 11) were transformed to the standard Johnson *V* magnitude after Harmanec (1998), using the all-sky $B-V$ and $U-B$ indices of all three stars derived at Hvar.

Finally, the Geneva 7-C all-sky observations (dataset 13) were transformed to the standard *UBV* system using the transformation formulæ devised by Harmanec & Božić (2001). All mean *UBV* values for individual datasets thus obtained are summarised in Table C.1 to illustrate the accuracy, with which the conversion to one system was possible.

In Figure C.1 we also plot all homogenised yellow observations vs. time. There are probably still some minor zero-point differences between individual data sets (APT photometry in on the instrumental system, which, however seems to be rather stable in time; Guinan - priv.com.). The plot in the bottom panel of Fig. C.1 is indicative of some small secular variations but such a statement would require verification through differential observations relative to some other comparison than HR 96.

[3] The program suite with a detailed manual is available at http://astro.troja.mff.cuni.cz/ftp/hec/PHOT/

Table A.2. Individual SPEFO RVs of V746 Cas for Hα and He I 6678 Å and Gaussian RVs for the He I 6678 Å line. RVs of the line cores and line outer wings are tabulated separately. All RVs are in km s^{-1}.

RJD	Hα 6563 Å SPEFO		He I 6678 Å SPEFO		He I 6678 Å Gauss		Spg.
	core	wings	core	wings	core	wings	No.
52538.5637	−13.14 ± 2.52	−19.65 ± 0.54	−15.04 ± 0.34	−17.02 ± 3.07	−12.	−21.	7
53025.2936	−10.82 ± 0.46	2.96 ± 0.77	−8.05 ± 0.45	−7.01 ± 2.17	−9.	6.	7
53026.2813	−9.05 ± 0.26	7.35 ± 1.17	−6.99 ± 0.90	9.70 ± 2.50	−9.	9.	7
56175.5586	−13.57 ± 0.58	−6.36 ± 0.84	−1.28 ± 0.09	−8.41 ± 1.19	1.35	−0.35	8
56176.5910	−14.05 ± 0.11	−4.63 ± 0.28	−2.64 ± 0.29	8.76 ± 2.46	−4.49	7.01	8
56177.5783	−11.79 ± 0.27	1.81 ± 0.39	−5.04 ± 0.87	11.77 ± 1.14	−2.04	14.46	8
56178.5868	−8.67 ± 0.73	8.80 ± 0.43	3.22 ± 0.33	24.27 ± 0.18	−4.02	24.58	8
56179.5853	−11.32 ± 0.06	9.86 ± 0.93	3.87 ± 0.32	28.02 ± 0.57	−0.97	27.03	8
56182.6157	−10.95 ± 0.42	14.17 ± 1.35	−3.48 ± 0.21	33.54 ± 0.24	−10.93	37.97	8
56188.5120	−12.62 ± 0.40	−28.60 ± 1.05	−5.19 ± 0.13	−25.18 ± 1.09	1.00	−20.30	8
56190.5364	−18.99 ± 0.15	−32.92 ± 2.36	−6.94 ± 0.07	−46.13 ± 1.60	0.66	−37.74	8
56202.5101	−12.70 ± 0.52	−1.29 ± 0.79	2.72 ± 0.48	0.10 ± 0.62	−0.51	9.39	8
56203.5069	−7.94 ± 0.10	3.02 ± 0.46	4.54 ± 1.13	7.90 ± 2.05	6.27	15.87	8
56204.5150	−10.05 ± 0.23	3.10 ± 0.52	5.51 ± 0.51	12.84 ± 0.82	3.75	15.95	8
56213.5446	−13.00 ± 0.18	−8.46 ± 0.68	−4.81 ± 0.14	0.97 ± 0.39	−9.08	−2.38	8
56214.4187	−16.90 ± 0.24	−16.45 ± 1.62	−7.63 ± 0.37	−18.19 ± 0.70	−4.99	−18.69	8
56746.6501	−7.21 ± 0.64	−4.74 ± 0.91	−2.85 ± 0.46	−6.82 ± 0.79	11.	−4.	9
56764.5933	−4.98 ± 0.63	7.51 ± 0.61	6.80 ± 0.35	20.45 ± 1.87	2.	10.	9
56765.5438	7.03 ± 0.18	9.85 ± 3.35	15.41 ± 0.75	16.45 ± 1.64	20.	17.	9
56772.5422	−14.23 ± 0.35	−7.02 ± 0.30	−4.75 ± 0.62	−8.20 ± 0.79	−2.	−11.	9
56782.5181	−10.29 ± 0.77	−22.95 ± 2.54	−2.33 ± 1.83	−40.34 ± 0.79	7.	−31.	9
56810.5577	−8.21 ± 1.68	−16.29 ± 0.35	1.35 ± 1.04	−14.02 ± 0.17	7.	−22.	9
56816.5317	−1.52 ± 1.93	6.57 ± 4.13	15.81 ± 0.52	14.13 ± 0.71	11.	21.	9
56817.4931	3.45 ± 0.47	9.78 ± 3.35	−5.16 ± 0.30	35.79 ± 1.30	−5.	18.	9
56819.4233	−0.80 ± 2.20	3.59 ± 6.15	16.24 ± 4.58	28.33 ± 1.20	12.	10.	9
56822.4782	−14.71 ± 0.30	−7.68 ± 0.63	−4.34 ± 0.35	−3.65 ± 2.58	−4.	6.	9
56826.3772	−30.03 ± 0.47	−37.24 ± 1.61	−6.01 ± 0.17	−49.38 ± 1.67	3.	−50.	9
56827.4581	−21.99 ± 0.53	−40.63 ± 4.52	−11.58 ± 1.04	−73.09 ± 0.96	−2.	−55.	9
56851.3742	−23.96 ± 1.22	−39.08 ± 4.04	−10.51 ± 0.52	−45.58 ± 0.62	−2.	−46.	9
56852.4071	−28.71 ± 0.18	−34.69 ± 1.33	−21.05 ± 0.52	−55.09 ± 0.17	−20.	−47.	9
56852.4657	−22.29 ± 3.96	−33.37 ± 1.10	−31.67 ± 0.30	−58.98 ± 1.48	−22.	−48.	9
56856.5629	−25.75 ± 0.47	−30.15 ± 0.81	−3.30 ± 0.46	−52.72 ± 0.79	16.	−44.	9
56861.4063	−20.57 ± 0.47	−9.85 ± 0.35	1.69 ± 0.35	−8.86 ± 0.46	−3.	−9.	9
56866.4436	−20.86 ± 0.30	8.51 ± 2.37	−13.05 ± 0.35	15.47 ± 1.21	−9.	7.	9
56889.3848	−17.08 ± 0.18	−1.60 ± 1.40	4.38 ± 0.37	8.01 ± 0.30	4.	1.	9
56910.3387	−15.09 ± 3.96	−19.84 ± 2.79	−9.13 ± 0.91	−26.24 ± 1.21	−8.	−18.	9
56920.3238	16.22 ± 1.84	18.33 ± 1.23	–	–	−−	−−	9
56928.3090	−17.42 ± 0.13	−35.75 ± 0.83	−13.61 ± 0.33	−54.56 ± 0.96	−6.	−47.	9
56949.2711	−10.92 ± 0.30	2.62 ± 2.31	−2.68 ± 0.35	16.15 ± 1.48	−16.	22.	9
56950.2946	−15.20 ± 0.18	−12.03 ± 0.70	−13.94 ± 0.69	−13.77 ± 3.89	−15.	−9.	9
56978.2935	−14.62 ± 0.35	−33.26 ± 0.53	−24.65 ± 0.79	−34.15 ± 1.13	−19.	−26.	9
57073.2605	−5.56 ± 0.47	5.16 ± 2.13	−6.07 ± 0.17	21.75 ± 1.58	−2.	13.	9
57073.3662	−2.40 ± 0.52	6.57 ± 1.33	10.02 ± 1.05	20.56 ± 0.60	9.	12.	9
57074.2706	−4.87 ± 0.53	6.38 ± 0.35	5.43 ± 0.60	20.80 ± 0.35	2.	9.	9
57110.2598	−9.36 ± 2.54	−35.20 ± 0.98	−11.44 ± 5.81	−47.73 ± 1.65	−2.	−53.	9
57123.6370	−4.86 ± 0.30	11.32 ± 0.77	5.53 ± 0.75	10.71 ± 1.73	3.	11.	9
57137.6098	−4.08 ± 1.23	−25.18 ± 0.88	−14.59 ± 0.62	−23.40 ± 1.25	−13.	−23.	9
57154.5792	−12.83 ± 0.47	−18.28 ± 0.18	−4.78 ± 0.86	−24.82 ± 0.79	1.	−18.	9
57228.4145	10.53 ± 0.63	−13.12 ± 3.26	3.76 ± 2.17	–	−−	−−	9
57256.4904	−19.43 ± 0.18	−26.81 ± 2.16	−5.85 ± 0.75	−30.56 ± 0.46	1.	−7.	9
57260.5354	−22.76 ± 1.06	−39.29 ± 0.88	−20.31 ± 1.99	−51.07 ± 1.87	−6.	−44.	9
57277.3647	−3.11 ± 2.65	16.58 ± 0.77	20.21 ± 0.60	26.43 ± 1.08	11.	24.	9
57295.4332	−9.01 ± 0.98	7.60 ± 1.24	−7.86 ± 0.87	21.81 ± 1.34	−13.	18.	9
57300.3763	−2.03 ± 0.47	9.22 ± 1.85	3.64 ± 0.35	14.87 ± 1.99	−3.	12.	9
57308.3352	−13.20 ± 1.76	−19.88 ± 2.30	−9.18 ± 1.13	−23.01 ± 4.22	−8.	−28.	9
57328.2087	−8.13 ± 3.26	6.11 ± 0.47	−5.12 ± 0.75	13.71 ± 0.46	−10.	6.	9
57328.6913	−4.37 ± 0.18	8.11 ± 1.85	2.34 ± 1.21	29.29 ± 1.21	−3.	20.	9

Table C.1. Individual photometries of V746 Cas and its comparison stars transformed to the standard Johnson *UBV* system

Dataset	Star	No. of obs.	V (mag.)	B (mag.)	U (mag.)	$B-V$ (mag.)	$U-B$ (mag.)	Source
14A	HR 96	23	5.748(10)	5.680(10)	5.369(21)	−0.068	−0.311	D
14A	HD 567	8	7.215(06)	7.188(23)	6.789(07)	−0.027	−0.399	D
14A	V746 Cas	6	5.601(04)	5.486(06)	4.891(05)	−0.115	−0.595	D
14D	HD 567	11	7.224(12)	7.194(22)	6.805(14)	−0.029	−0.389	D
14D	V746 Cas	6	5.606(05)	5.489(04)	4.901(05)	−0.117	−0.588	D
11	HR 96	157	5.737(05)	–	–	–	–	A
11	HD 567	8	7.206(09)	–	–	–	–	A
11	V746 Cas	6	5.590(10)	–	–	–	–	A
12	V746 Cas	1635	5.606(01)	–	–	–	–	B
12	HD 567	847	7.235(01)	–	–	–	–	B
13	V746 Cas	251	5.586(09)	5.475(11)	4.879(13)	−0.111	−0.596	E

Notes. *Column "Dataset":* 11...All-sky Hipparcos H_p observations, transformed to Johnson V after Harmanec (1998); 12...Differential *uvby* observations secured with the Four College Automatic Reflector relative to HR 96 = HD 2054. Also the check star HD 567 = BD+51°12 was regularly observed.; 13...All-sky Geneva 7-C observations secured with the Mercator Telescope at LaPalma; 14A...Hvar all-sky photometry; 14D.. Hvar differential photometry relative to HR 96.
Column "Source": A...Perryman & ESA (1997); B...Dukes et al. (2009) and this paper; C...De Cat et al. (2004); D...this paper.

The reason for the above statement is that the primary comparison HR 96 = HD 2054 is suspected to be a CP star and it was found to be a spectroscopic binary with a $48\overset{d}{.}2905$ period (Hube 1983). Using the program `FOTEL`, we re-analysed available radial velocities, namely 2 RVs from old David Dunlap Observatory (DDO) prismatic 33 Å mm^{-1} spectra (Hube 1983), 4 RVs from the DDO 40 Å mm^{-1} grating-spectrograph spectra (Hube 1970), 5 RVs from Herstmonceux (HRM) Yapp-reflector prismatic 70-173 Å mm^{-1} spectra (Palmer et al. 1968), and 25 RVs from the Dominion Astrophysical Observatory (DAO) 15 Å mm^{-1}grating spectra (Hube 1983). We weighted individual RVs by the weights inversely proportional to their rms errors and then also applied similar external weights for individual spectrographs. Unlike Hube (1983) we allowed for the determination of individual systemic γ velocities for the four individual spectrographs. Our solution is compared with that of Hube (1983) in Table C.2

In Figure C.2 we show a plot of the Hipparcos H_p photometry transformed to Johnson V magnitude vs. phase of the $48\overset{d}{.}29$ orbital period of HR 96. One can suspect the presence of a small-amplitude variation with a minimum near the superior conjunction of the binary. This can naturally further complicate the period analysis of the photometry of V746 Cas.

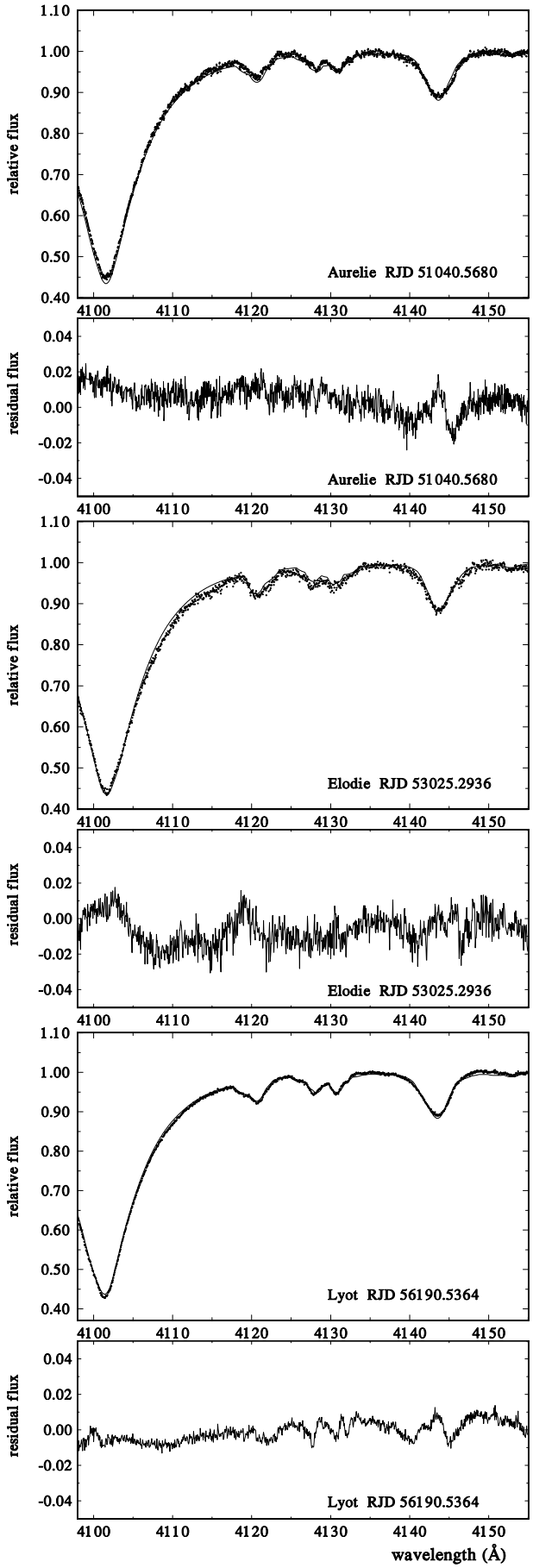

Fig. B.1. The fit of several observed spectra (dots) by interpolated synthetic spectra (lines) for the region covered also by the Aurelie spectra is shown. The residuals from the fits are also shown below each spectrum (note the enlarged scale used for the flux units).

Table A.4. RVs of all high-resolution spectra of V746 Cas derived with the help of PYTERPOL program. **The RVs and their errors were estimated with the help of the MCMC silulation.**

RJD	RV (km s^{-1})	Spg.
51005.5778	−44.08 ± 5.28	6
51006.5970	−65.14 ± 7.46	6
51007.5940	−69.06 ± 7.30	6
51009.5946	−61.16 ± 4.96	6
51010.5765	−63.94 ± 6.48	6
51011.5748	−52.72 ± 5.65	6
51012.5773	−36.68 ± 2.90	6
51036.6214	−47.29 ± 4.06	6
51038.4965	−33.29 ± 2.61	6
51040.5680	−20.27 ± 2.36	6
51042.6335	−1.75 ± 2.89	6
51094.4222	0.95 ± 2.44	6
51096.5979	6.86 ± 2.07	6
51097.5923	16.16 ± 1.81	6
51098.4748	18.41 ± 2.84	6
51099.4536	15.20 ± 3.48	6
52538.5637	−18.88 ± 0.81	7
53025.2936	6.95 ± 1.34	7
53026.2813	14.11 ± 1.74	7
56175.5586	−6.88 ± 0.49	8
56176.5910	−3.13 ± 0.72	8
56177.5783	4.25 ± 0.91	8
56178.5868	13.33 ± 1.16	8
56179.5853	15.20 ± 1.35	8
56182.6157	23.57 ± 1.64	8
56188.5120	−18.24 ± 1.79	8
56190.5364	−45.88 ± 1.93	8
56202.5101	−3.22 ± 0.85	8
56203.5069	1.68 ± 1.51	8
56204.5150	7.50 ± 1.03	8
56213.5446	−11.10 ± 1.06	8
56214.4187	−25.50 ± 1.13	8

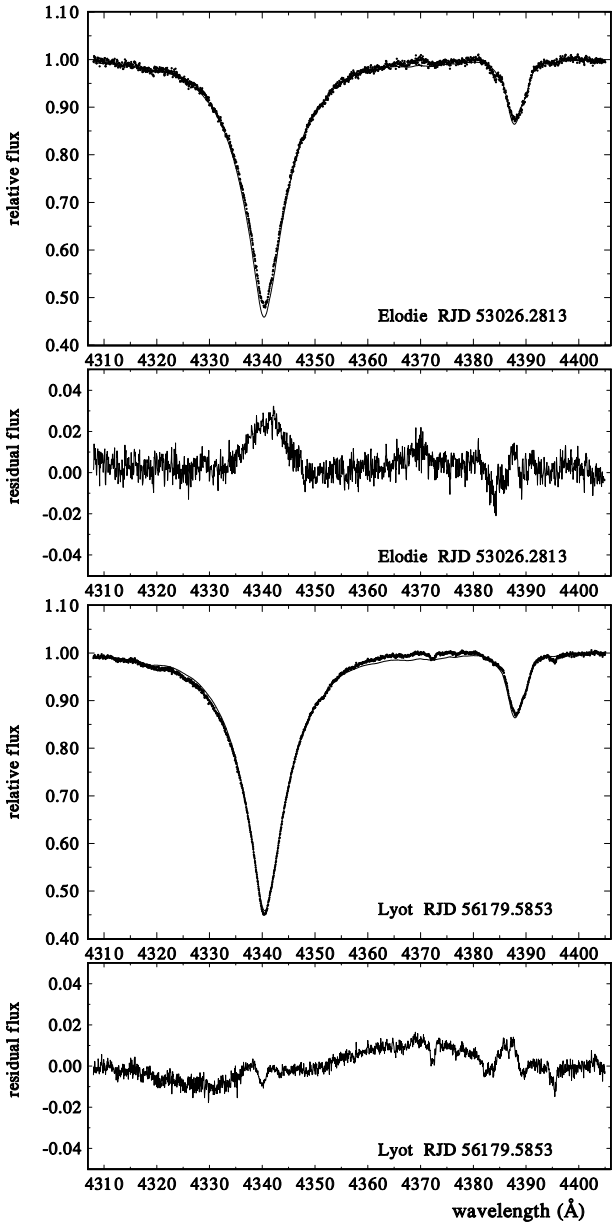

Fig. B.2. The same as Fig. B.1 for the neighbourhood of the Hγ line.

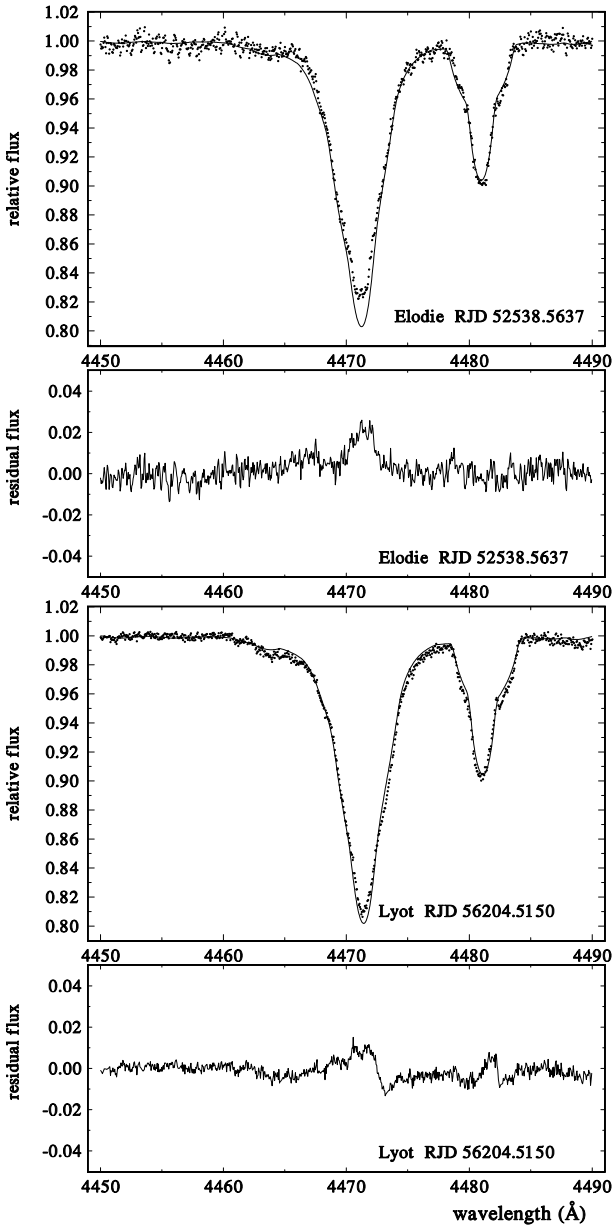

Fig. B.3. The same as Fig. B.1 for the neighbourhood of the H I 4472 Å and Mg II 4481 Å lines.

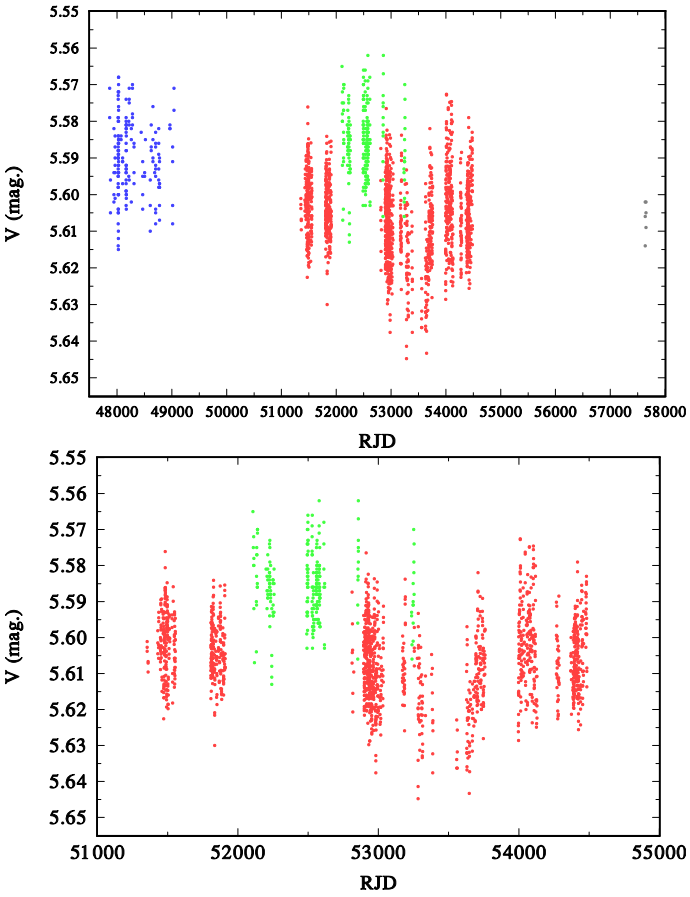

Fig. C.1. *Top:* A time plot of V photometry of V746 Cas vs. time for the four datasets available. They are distinguished as follows: blue... all-sky H_p magnitudes transformed to Johnson V; red... differential Strömgren y magnitude relative to the Hvar all-sky V magnitude of $5^m.748$ for HR 96; green... Johnson V magnitude transformed from the all-sky Geneva 7-C observations; grey... standard differential Johnson V magnitude relative to HR 96 secured at Hvar. *Bottom:* An enlarged part of the plot for the time interval, where the y and Geneva transformed V magnitudes overlap.

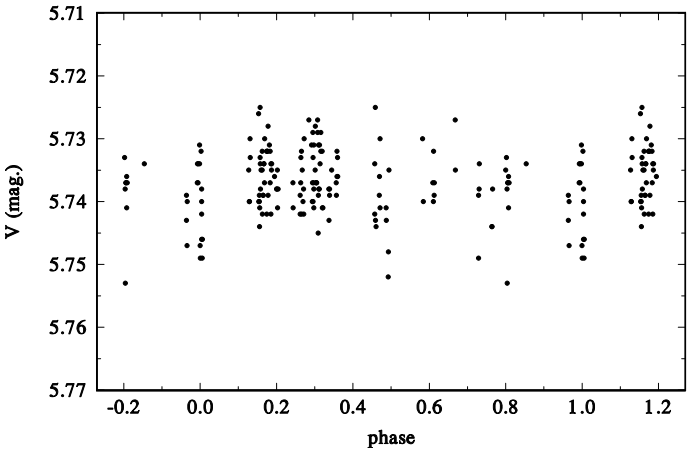

Fig. C.2. The light curve of Hipparcos photometry of HR 96 transformed to Johnson V plotted for the ephemeris of the spectroscopic binary orbit $T_{\text{super.conj.}}$ = RJD 45260.24 + $48^d.2884$.

Table C.2. Orbital solutions for the comparison star HR 96.

Element	Hube (1983)	Our new
P (d)	48.2905(42)	48.2884(15)
$T_{\text{periastr.}}$	45248.12(60)*)	45248.29(35)
$T_{\text{super.c.}}$	45260.12	45260.24
$T_{\text{RVmax.}}$	45250.43	45250.58
e	0.384(29)	0.376(25)
ω (deg.)	320.0(6.8)	321.0(2.9)
K_1 (km s^{-1})	30.1(1.0)	29.02(74)
$\gamma_{\text{DDO old}}$ (km s^{-1})	–	+9.37(56)
γ_{HRM} (km s^{-1})	–	+1.8(2.6)
$\gamma_{\text{DDO new}}$ (km s^{-1})	–	−0.23(39)
γ_{DAO} (km s^{-1})	+3.41(74)	+3.22(73)
rms (km s^{-1})	not given	2.10
No. of RVs	25	36

Notes. *) The epoch given by Hube (1983), 45240.60(60) is an obvious misprint and cannot reproduce the phase plot in his Fig. 1. We quote his period with error derived also from all 36 RVs, which he fixed in the above reproduced solution based on the DAO RVs only.
All epochs are in RJD; rms is the rms of 1 observation of unit weight.